Atmos. Chem. Phys. Discuss., 15, 11409–11464, 2015
www.atmos-chem-phys-discuss.net/15/11409/2015/
doi:10.5194/acpd-15-11409-2015

Atmospheric Chemistry and Physics Discussions
Open Access

Quantifying the contribution of long-range transport to Particulate Matter (PM) mass loadings at a suburban site in the North-Western Indo Gangetic Plain (IGP)

H. Pawar[1], S. Garg[1], V. Kumar[1], H. Sachan[1], R. Arya[1,2], C. Sarkar[1], B. P. Chandra[1], and B. Sinha[1]

[1]Department of Earth and Environmental Sciences, Indian Institute of Science Education and Research Mohali, Sector 81, S.A.S Nagar, Manauli PO, Punjab 140306, India
[2]School of Chemical and Biomolecular Engineering, Cornell University, Ithaca, New York, USA

Received: 22 January 2015 – Accepted: 30 March 2015 – Published: 17 April 2015

Correspondence to: B. Sinha (bsinha@iisermohali.ac.in)

Published by Copernicus Publications on behalf of the European Geosciences Union.

Abstract

Many sites in the densely populated Indo Gangetic Plain (IGP) frequently exceed the national ambient air quality standard (NAAQS) of 100 µg m^{-3} for 24 h average PM_{10} and 60 µg m^{-3} for 24 h average $PM_{2.5}$ mass loadings, exposing residents to hazardous levels of PM throughout the year.

We quantify the contribution of long range transport to elevated PM levels and the number of exceedance events through a back trajectory climatology analysis of air masses arriving at the IISER Mohali Atmospheric Chemistry facility (30.667° N, 76.729° E; 310 m a.m.s.l.) for the period August 2011–June 2013. Air masses arriving at the receptor site were classified into 6 clusters, which represent synoptic scale air mass transport patterns and the average PM mass loadings and number of exceedance events associated with each air mass type were quantified for each season.

Long range transport from the west leads to significant enhancements in the average coarse mode PM mass loadings during all seasons. The contribution of long range transport from the west and south west (Source region: Arabia, Thar desert, Middle East and Afghanistan) to coarse mode PM varied between 9 and 57 % of the total $PM_{10-2.5}$ mass. Local pollution episodes (wind speed < 1 m s^{-1}) contributed to enhanced coarse mode PM only during winter season. South easterly air masses (Source region: Eastern IGP) were associated with significantly lower coarse mode PM mass loadings during all seasons.

For fine mode PM too, transport from the west usually leads to increased mass loadings during all seasons. Local pollution episodes contributed to enhanced $PM_{2.5}$ mass loadings during winter and summer season. South easterly air masses were associated with significantly lower $PM_{2.5}$ mass loadings during all seasons. Using simultaneously measured gas phase tracers we demonstrate that most $PM_{2.5}$ originated from combustion sources.

ACPD
15, 11409–11464, 2015

Contribution of long-range transport to PM mass loading in the NW-IGP

H. Pawar et al.

The fraction of days in each season during which the PM mass loadings exceeded the national ambient air quality standard was controlled by long range transport to a much lesser degree.

For the local cluster, which represents regional air masses (Source region: NW-IGP), the fraction of days during which the national ambient air quality standard (NAAQS) of 60 µg m^{-3} for 24 h average $PM_{2.5}$ was exceeded, varied between 22 % of the days associated with this synoptic scale transport during monsoon season and 85 % of the days associated with this synoptic scale transport during winter season; the fraction of days during which the national ambient air quality standard (NAAQS) of 100 µg m^{-3} for the 24 h average PM_{10} was exceeded, varied between 37 % during monsoon season and 84 % during winter season.

Long range transport was responsible for both, bringing air masses with a significantly lower fraction of exceedance days from the Eastern IGP and air masses with a moderate increase in the fraction of exceedance days from the West (Source region: Arabia, Thar desert, Middle East and Afghanistan).

In order to bring PM mass loadings in compliance with the national ambient air quality standard (NAAQS) and reduce the number of exceedance days, mitigation of regional pollution sources in the NW-IGP needs to be given highest priority.

1 Introduction

India is a rapidly developing nation. Population growth, urbanization and industrial development have led to increasing emissions, resulting in particulate matter (PM) mass loadings that frequently exceed the national ambient air quality standard (NAAQS) of 100 µg m^{-3} for 24 h average PM_{10} and 60 µg m^{-3} for 24 h average $PM_{2.5}$ mass loadings. This exposes the residents to hazardous levels of PM throughout the year.

Daily particulate matter mass loadings show a clear correlation with daily mortality and morbidity from respiratory and cardio vascular diseases (Englert, 2004; Kappos et al., 2004; Pope and Dockery, 2006). The correlation between extreme PM mass

ACPD
15, 11409–11464, 2015

loadings and mortality has been recognized early in the history of air pollution research (Firket, 1931; Schrenk et al., 1949; Nemery et al., 2001) and the predicted disaster of the “London Fog” (Logan, 1953; Bell and Davis, 2001) resulted in first efforts to combat PM air pollution through legislation and regulatory intervention. However, the effect of moderate to low PM mass loadings on human health was recognized much later (Shy, 1979; Ware et al., 1981; Dockery et al., 1989, 1993; Schwartz, 1994; Pope et al., 1995; Pope, 2000) and the accumulated evidence has resulted in a revision of the air quality standards in many countries including India (NAAQS, 2009).

Many sites in the densely populated IGP are in violation of the NAAQS throughout the year except during the monsoon season, when removal through wet scavenging brings PM levels into compliance. Enhanced PM is associated with increased hospital visits/admission of patients with respiratory symptoms and increased mortality (Mohanraj and Azeez, 2004; Nag et al., 2005; Pandey et al., 2005; Kaushik et al., 2006). The complex interplay of natural windblown dust, trans-boundary air pollution and local sources impose severe challenges on the Central Pollution Control Board, the local regulatory body in charge of enforcing the NAAQS. While it is clearly inappropriate to blame individual industrial units for natural windblown dust or trans-boundary air pollution, the contribution of these two factors to extreme events should not be used as an excuse to avoid all regulatory action. This study seeks to quantify the effect of long range transport of both natural windblown dust and anthropogenic PM to the regional background PM mass loadings and to establish a baseline against which the enhancement due to local sources can be measured.

Back trajectory models use archived meteorological data and allow for the identification of source regions of pollutants measured at a receptor site. Air mass trajectories are defined as the path of an infinitesimally small air parcel. Back trajectories trace the air mass back in time and describe where the air mass reaching a receptor site originated.

Statistical analysis of large datasets of air mass back trajectories has been a popular tool for identifying source regions of particulate matter. Such statistical analysis attributes all changes in particulate matter mass loading at a receptor site to spatially fixed sources and seeks to identify those sources by investigating the statistical correlation between air mass origin and the particulate mass loadings observed at the receptor site. While wind rose or pollution rose plots are most appropriate to identify local sources (Fleming, 2012), statistical analysis of a large set of back trajectories (Stohl, 1996, 1998) has been a popular tool for identifying distant source regions of particulate matter (Borge et al., 2007; Abdalmogith and Harrison, 2005; Nyanganyura, 2008; Buchanan et al., 2002) and investigating trans-boundary particulate matter pollution (Miller et al., 2010; Grivas et al., 2008; Borge et al., 2007). Cluster analysis is a multivariate statistical technique that splits the data into a number of groups while maximizing the homogeneity within each group and maximizing the distance between groups.

The aim of the present study is to better understand the conditions under which PM mass loadings exceeding the national ambient air quality standard (NAAQS) of $100\,\mu g\,m^{-3}$ for 24 h average PM_{10} and $60\,\mu g\,m^{-3}$ for 24 h average $PM_{2.5}$ (NAAQS, 2009) occur in the North West Indo Gangetic Plain (NW-IGP) and to quantify the contribution of long range transport to those exceedance events. Here, we quantify the contribution of long range transport to fine ($PM_{2.5}$) and coarse ($PM_{10-2.5}$) particulate matter (PM) using back trajectory cluster analysis, pinpoint potential source regions of enhanced background PM mass loadings and further attempt to constrain the origin of the particulate matter by correlating the observations with those of gas phase combustion tracers (CO, NO_2, benzene and acetonitrile). We analyse a two year dataset (August 2011 till June 2013) measured at the Atmospheric Chemistry facility of the Indian Institute for Science Education and Research (IISER) Mohali.

ACPD
15, 11409–11464, 2015

2 Materials and methods

2.1 Study location, air quality data and general meteorology

We use two years (August 2011 till June 2013) of hourly data of fine ($PM_{2.5}$) and coarse ($PM_{10-2.5}$) particulate matter (PM) and gas phase combustion tracers (CO, NO_2, benzene and acetonitrile) measured at the Atmospheric Chemistry facility of the Indian Institute of Science Education and Research Mohali. The facility, the measurement techniques used, data coverage and data quality assurance protocols are described in great detail in Sinha et al. (2014), hence only a brief description is provided here. Particulate matter (PM_{10} and $PM_{2.5}$) mass concentrations were measured using separate Thermo Fischer Scientific 5014i beta continuous ambient particulate monitors working on the principle of beta attenuation, NO_2 measurements were performed by chemiluminescence technique using a Thermo Fischer Scientific 42i trace level analyser, Carbon monoxide (CO) was measured by gas filter correlation (GFC) non dispersive infrared (NDIR) technique using Thermo Fischer Scientific 48i trace level enhanced analyser and the mixing ratios of benzene and acetonitrile were determined using a high sensitivity proton transfer reaction quadrupole mass spectrometer (HS Model 11-07HS-088; Ionicon Analytik Gesellschaft, Austria).

Figure 1 shows the location of city Mohali in the north-west Indo-Gangetic plain in the Indian state Punjab, close to the forested slopes of the foothills of the Himalayan mountain range on the left side. The measurement facility is located at a suburban site, south west of the city centre of the "tri-city" – an urban agglomeration of the three cities Chandigarh, Mohali and Panchkula – inside the residential campus of IISER Mohali (30.667° N, 76.729° E, 310 m a.m.s.l.). On the right side, Fig. 1 shows a close up illustrating the exact location of the measurement facility and its spatial relationship with respect to the nearby cities and potential local point sources of particulate matter and the mountain range.

Figure 2 shows wind rose plots for winter (December–February), summer (March–June), monsoon (July–September) and post-monsoon (October and November) sea-

ACPD
15, 11409–11464, 2015

son. Most air masses impacting the site travel parallel to the mountain range and reach the facility from north-western or south-eastern direction. Periods of calm (wind speed $< 1\,\mathrm{m\,s^{-1}}$) account for only 4.5, 2.5, 5.2 and 8.7 % of the total time during winter, summer, monsoon, post-monsoon season respectively and slow transport (wind speed 1–$5\,\mathrm{m\,s^{-1}}$) was observed 64.1, 48.7, 56.1 and 71.4 % of the total time, respectively. The high frequency with which rapid transport of air masses towards the facility (wind speed $> 5\,\mathrm{m\,s^{-1}}$) was observed (31.4, 48.8, 38.7 and 19.9 % of the total time during winter, summer, monsoon, post-monsoon season respectively) indicates that long range transport potentially plays a significant role in determining pollutant loadings at the site. The general meteorology of the site is as follows.

During winter season, weak northerlies or north-westerlies and a weak, low-level anti-cyclonic circulation prevails in the NW-IGP. Wintertime fog occurs frequently and is favoured by subsidence of air masses over the IGP, low temperatures, high relative humidity and low wind speeds ($< 5\,\mathrm{m\,s^{-1}}$). Sporadic winter rains are generally associated with the western disturbance (Pisharoty and Desai, 1956; Agnihotri and Singh, 1982; Mooley, 1957; Dimri, 2004). The western disturbance is a terrain-locked low-pressure system that forms when an upper-level extra tropical storm originating over the Mediterranean passes over the notch formed by the Himalayas and Hindu Kush mountains. The resulting notch depression is small, five degrees latitude/longitude in size, and develops within an existing trough in the belt of subtropical westerly wind. South-westerly wind ahead of the trough brings moisture from the Arabian Sea, which encounters the Western Himalayas that lie almost normal to this moist wind. Part of the wind is channelled into the IGP which subsequently reach the receptor site from the southeast. Fast westerly winds in winter are typically associated with a strong subtropical jet stream poised over westerly troughs.

During summer season, the prevailing wind direction is north-westerly. Tropospheric subsidence over north-western India due to the "heat low" associated with westerly flow across Afghanistan and Pakistan, channels air masses originating in the Middle East into the IGP. The boundary layer, experiences a strong temperature inversion (Das,

Discussion Paper | Discussion Paper | Discussion Paper | Discussion Paper |

ACPD

15, 11409–11464, 2015

Contribution of long-range transport to PM mass loading in the NW-IGP

H. Pawar et al.

1962) due to dust induced cooling in the upper layers. The resulting steep horizontal pressure gradient is responsible for strong surface winds that carry dust and sand storms (Bryson and Swain, 1981). These loo-winds are extremely hot and dry. During April, the centre of the subtropical jet stream is located over Northern India and gives rise to cold subtropical westerlies in the upper troposphere. At the same time the lower troposphere reaches very high temperatures due to quick response of the land to the overhead sun. This favours severe thunderstorms with strong squalls at the leading edge of the downdraft during summer season. Such thunderstorms can cause convective dust storms, locally known as "Aandhi" (Ramaswamy, 1956; Joseph, 1982). In March and April, south-easterly winds are generally associated with the western disturbance. The climatology of the western disturbance shows a significant inter-annual variability, as it is correlated with the Polar/Eurasia tele-connection pattern. A weak circumpolar vortex can lead to an enhancement in the number of notch depressions and late "winter storms" in March and April (Lang and Barros, 2004). South-easterly winds in June are generally associated with an earlier than usual onset of the monsoon. In normal years the monsoon reaches Punjab in the first week of July.

During monsoon season, the surface heat low located over the Pakistan region and the monsoon trough stretching from the North-West IGP to the Bay of Bengal dominate the general circulation over the IGP. The strength and position of the monsoon trough drives the "active-break" cycles of the rains on the intra-seasonal scale (Sikka and Gadgil, 1980; Goswami, 1998; Goswami et al., 2006a, b). During "active" spells the trough is located over south or central India and cyclonic swirls form all across the trough. The prevailing wind direction during active spells is south-easterly. During "break" spells the trough is located over the foothills of the Himalayas, the low level jet originating off the coast of Somalia enters the IGP through the Indus valley (Joseph and Raman, 1966). Cyclonic swirls are mostly absent and rains are suppressed everywhere except over the foothills (Joseph and Sijikumar, 2004). During break spells of the monsoon circulation, the prevailing wind direction is north westerly. Break spells are associated with lower-tropospheric inversions, dusty winds and lower troposphere

ACPD
15, 11409–11464, 2015

anti-cyclonic vorticity over the IGP (Sikka, 2003; Rao and Sikka, 2005; Bhat, 2006). Most rainfall events occur during the "active spells" when the wind direction is south-easterly. However, occasional night time rainfall events are observed even during break spells in Punjab.

During post monsoon season, the prevailing wind direction is north-westerly. The retreating monsoon brings subsidence of dry Central Asian air masses over the North-west IGP. In particular during night time, katabatic winds reach the receptor site from the northern to eastern wind sector. Winds are generally weak; the wind speed is less than $5\,m\,s^{-1}$ for more than 80 % of the time.

Since the purpose of this study is to investigate the contribution of long range transport to PM pollution we restricted our analysis to measurements obtained between 12 to 4 p.m. LT (UTC + 05:30) during the day and 3 to 6 a.m. LT (UTC + 05:30) at night and consider calm conditions with wind speeds of less than $1\,m\,s^{-1}$ separately.

The daytime period was selected, because the local daytime boundary layer reaches its maximum height around 2 p.m. and the contribution of long range transport to PM is highest in the time period centred on this time.

The night time period was selected because the contribution of local sources, in particular the contribution of local traffic, construction activity and biomass combustion to air pollution is least during late night and early morning hours.

Figure 3 shows that both fine mode PM ($PM_{2.5}$, bottom panels) and coarse mode PM ($PM_{10-2.5}$, top panels) show a bimodal distribution with a peak in the morning and the evening due to local traffic and biomass combustion emissions and a low in the mid-day hours and the early morning hours during all seasons (Fig. 3). The bimodal behaviour is most pronounced during post monsoon season, when low wind speeds prevail and local and regional sources dominate the aerosol mass loading. The bimodal behaviour is weakest during monsoon season when active convection and high wind speeds reduce the influence of local sources. Fine mode PM shows the lowest mass loadings during mid-day, when the boundary layer is highest, while coarse mode PM shows the lowest mass loadings in the early morning hours.

ACPD
15, 11409–11464, 2015

During summer and monsoon season, there is a pronounced difference between mean and median coarse mode PM loadings. This discrepancy is caused by the contribution of episodic events (dust storms) to coarse mode PM in both seasons. For our back trajectory analysis, we calculated the median PM mass loading (see the Supplement) and gas phase mixing ratio of CO, benzene and acetonitrile for the period in question. For rainfall we provided the sum (total precipitation in the time window in question) rather than the median, as we consider the total rainfall a better indicator of wet scavenging.

2.2 Back trajectory modeling

We computed three day (72 h) backward trajectories using HYSPLIT_ 4 (HYbrid Single Particle Lagrangian Integrated Trajectory) model in ensemble mode using National Oceanic and Atmospheric Administration's Global Data Acquisition System meteorology (Draxler and Rolph, 2013; Draxler and Hess, 1998) as input. We calculated ensemble runs for air masses arriving at the site (30.667° N, 76.729° E) at 20 m above the ground (the approximate sampling height for all instruments). The model was run twice daily with an arrival time of 09:00 UTC (2.30 p.m. local day-time) and 23:00 UTC (4.30 a.m. local night-time). Due to the close proximity of the site to the Himalayan mountain range the trajectory output was found to be very sensitive to the model's input data. IISER Mohali Air Quality station (30.667° N, 76.729° E) is located in the Indo-Gangetic Plain (IGP) at an altitude of 310 m a.m.s.l. approximately 20 km south west of the Shivalik hills, but the model's terrain height at the receptor site is 667.6 m a.m.s.l. for the GDAS dataset and 1249.9 m a.m.s.l. for the reanalysis dataset for a single trajectory arriving at the site. We calculated trajectory ensembles for our site using both datasets. The trajectory ensemble option starts multiple trajectories from the selected starting location. Each member of the trajectory ensemble is calculated by offsetting the meteorological data by a fixed grid factor (1 meteorological grid point in the horizontal and 0.01 sigma units in the vertical) which results in 27 trajectories. The model's terrain height varied between 200 and 3500 m a.m.s.l. for individual runs of the tra-

ACPD
15, 11409–11464, 2015

jectory ensemble for the GDAS dataset and between 240 and 5100 m a.m.s.l. for the reanalysis dataset. We conclude that the GDAS dataset performs better in modelling the terrain at our site and all further analysis in this work uses this dataset.

Out of the 27 trajectories in the ensemble run, only 3 trajectories are consistent with the measurement site, Mohali, being located in the plain (< 400 m a.m.s.l.) and Shimla, a mountain site 60 km NE of our site (Fig. 1) at 31.103° N, 77.172° E, being located in the mountains (> 400 m a.m.s.l.). We selected these three trajectories for further analysis.

Borge et al. (2007) have recently emphasised the importance of specifying adequate arrival heights for the outcome due to possible large variation in the wind speed and direction with height above the ground. Kassomenos et al. (2010), too, found a dependency of clustering outcome on the arrival heights of the trajectories. At our site, we find that the Himalayan mountain range acts as a great barrier and air masses are funnelled into the IGP. Consequently there is little dependency of the trajectory run outcome on arrival heights ≤ 500 m a.g.l., as long as the meteorological input data set represents the Himalayan mountain range topography adequately. The local wind direction observed at the site generally agrees with the wind vector at 10 m a.g.l. used in the GDAS dataset.

2.3 Back trajectory cluster analysis

Cluster analysis is a statistical method used to group data in large data sets into a small number of groups of similar data known as clusters. In this work we have used air masses' trajectory coordinates (time steps) as the clustering variables. A non-hierarchical method known as the *k* means procedure has been used in this study. The air mass back trajectories were subjected to *k* means clustering using a freeware called PAST (PAleontological STatistics). The number of clusters "*k*" is to be specified by the user prior to clustering. The assignment of back-trajectories to clusters is initially random. In an iterative procedure, trajectories are then moved to the cluster which has the closest cluster mean in Euclidean distance, and the cluster means are updated

ACPD
15, 11409–11464, 2015

accordingly (Bow, 1984). This process continues until the process of hopping from one cluster to another ceases. As a normal artefact of the k means clustering algorithm, the result is dependent upon the seed used for clustering (Kassomenos et al., 2010). Therefore, to get a robust result, clustering was initialized with 11 different trajectory orders and we selected the clustering result with the lowest root mean square difference for each predefined number of clusters.

The root mean square difference for an individual latitude and longitude value is given by

$$\text{RMSD} = \sqrt{(x_i - \bar{x})^2} + \sqrt{(y_i - \bar{y})^2} \tag{1}$$

where x_i and y_i stand for the latitude and longitude of the individual trajectory for a given hour and $\bar{x}$ and $\bar{y}$ for the cluster mean latitude and longitude of the same hour for the cluster to which that trajectory belongs. The total root mean square difference t-RMSD is the sum over all the RMSD values for a given set of back trajectories.

We selected the optimal number of clusters that best describe the different air–flow patterns to our site by computing the change in the minimum t-RMSD while increasing the number of clusters from n to $n+1$. This change in the minimum t-RMSD decreases abruptly as clusters of trajectories which are significantly different in terms of wind directions and speeds are separated from each other (Dorling et al., 1992). A threshold of 5 % change has been adopted (Brankov et al., 1998; Dorling et al., 1992) as an indication of the number of clusters to be retained.

3 Results and discussions

3.1 Optimization of the number of clusters

The number of clusters was optimized by minimizing the t-RMSD change for an increase in number of clusters, while retaining as few clusters as possible. Figure 4

ACPD
15, 11409–11464, 2015

shows the percent change in t-RMSD for a subsequent increase in number of clusters. The largest % decrease in t-RMSD is observed when the number of clusters is increased to 2 and subsequently 3. This corresponds to two major airflow corridors (southeasterly flow and westerly flow) and a local cluster. Increasing the number of clusters beyond this number allows splitting of the air masses in the western and southeastern corridor into several groups according to their transport speed and introduces a south westerly cluster. Initially, we identified the optimum number of clusters as seven, however, two of these seven clusters (fast north-westerly flow A and B) were classified into two different groups only, because for fast north-westerly flow "A" all three trajectories of the ensemble run showed equal transport speed while for fast north-westerly flow "B" two of the three trajectory solutions in the ensemble indicated slow air mass transport (trajectories arriving at 20 m a.g.l., Fig. 5) while one solution supported rapid transport (trajectory arriving at 250 m a.g.l., Fig. 5). Locally measured meteorological parameters indicated that both clusters are associated with hot dry "loo-winds" and dust storms during summer and above average wind speeds during other seasons. Therefore, both clusters were combined into one fast westerly cluster and the final number of optimum clusters was 6.

3.2 Spatial and dynamic patterns of the air flow associated with the clusters

Figure 6 shows the average trajectory of seven clusters identified by k means clustering superimposed on a land classification map (courtesy ESA GlobCover 2009 Project). The length of each mean trajectory is 3 days and the distance between two successive data points represents the 1 h interval. We find six distinct flow patterns, south easterly flow ($N = 263$), south westerly flow ($N = 79$), fast ($N = 78$), medium ($N = 83$) and slow ($N = 305$) westerly flow and a local cluster ($N = 556$). Figure 7a–f shows all the individual trajectories that contributed to each of the clusters, superimposed on a land classification map (courtesy ESA GlobCover 2009 Project). These plots give a qualitative impression of the variability of the flow within the individual clusters. Although considerable variability is observed between the individual trajectories contributing to each of

ACPD
15, 11409–11464, 2015

the clusters, in particular for the “local” cluster, each cluster of trajectories represents a distinct air mass fetch region. Figure 5 depicts the mean height (m a.g.l.) of the mean trajectories during the three days before their arrival at the receptor site. Trajectories from the slow, medium and fast westerly clusters descend from the free troposphere to reach the receptor site. Fast and medium westerly air masses show a rapid descent in the last 30 h prior to reaching the receptor site and are generally associated with high wind speeds, while slow westerly air masses display a gradual subsidence. The south easterly, south westerly and local cluster remain within the convective boundary layer throughout.

Figure 8 shows the temporal distribution of the air flows for the six clusters determined with respect to the different seasons and Table 1 presents the locally measured meteorological parameters for daytime/nighttime for each cluster and season.

The *local cluster* accounts for 40.1, 35.7, 31.1 and 51.3 % of the air mass trajectories during winter (December to February), summer (March to June), monsoon (July to September) and post-monsoon (October and November) season respectively. This air mass transport corresponds to times when weak northerlies or north-westerlies and a weak, low-level anti-cyclonic circulation prevail in the NW-IGP during winter, summer and post monsoon season. The predominant locally measured wind direction for this cluster during winter, summer and post monsoon season is west to north-west (47 % of the time) with katabatic winds (320–120° wind sector) accounting for most of the remainder (31 %). South easterly winds (8 %) and south westerly winds (14 %) account only for a minor fraction of the locally observed wind direction each. During summer season and monsoon season convective activity above the site is also attributed to this cluster. Strong squalls leading to “Aandhi” type convective dust storms (Joseph, 1982) are observed occasionally, both in late summer and early in the monsoon season. During monsoon season, locally observed wind direction associated with this cluster is variable (35 % north west, 29 % south east, 18 % south west, 18 % katabatic flow). The local cluster is associated with average temperatures and wind speeds at the lower end of those observed for the different clusters both during day and night in all seasons. The

ACPD
15, 11409–11464, 2015

absolute humidity is higher than the absolute humidity observed for medium and fast westerly flows and lower than the absolute humidity observed for south easterly and south westerly flow during all seasons. Occasionally rain events occur in all seasons, however, the total number of rain events associated with the local cluster is low except during monsoon season.

The *slow westerly* cluster is associated with the same general meteorology (weak northerlies or north-westerlies and a weak, low-level anti-cyclonic circulation) as the local cluster and most of the locally observed parameters are also similar to those of the local cluster. However, the fetch region of the air masses is larger. The predominant local wind direction for this cluster is west to northwest during all seasons including monsoon (50 %) and katabatic winds from the north-northwest to east-southeast sector (28 %) account for most of the remainder. South easterly winds (10 %) and south westerly winds (12 %) account only for a minor fraction of the locally observed wind direction each. The main differences between air masses associated with the local cluster and air masses associated with the slow westerly cluster are as follows: slightly higher temperatures and wind speeds are observed for the slow westerly cluster during most seasons and both relative and absolute humidity are lower for air masses associated with the slow westerly cluster due to the recent descend of the air masses from the free troposphere. Air masses associated with the slow westerly cluster have a shorter residence time in the convective boundary layer over the irrigated fields in the IGP and consequently contain less moisture. The slow westerly cluster accounts for 17.4, 26.6, 10.7 and 28.4 % of the air mass transport to the site during winter, summer, monsoon and post-monsoon season respectively. Rain events are associated with this cluster only rarely.

The *medium westerly* cluster is observed only during winter, summer and post monsoon seasons and accounts for 7.7, 8.5 and 4.5 % of the air masses respectively. The clusters are associated with a strong subtropical jet stream poised over westerly troughs and shows higher than average wind speeds. The predominant local wind direction for this cluster is west to northwest during all seasons (44 %) and katabatic

ACPD
15, 11409–11464, 2015

winds from the north-northwest to east-southeast sector (38 %) account for most of the remainder of the flow. South westerly (13 %) and south easterly winds (6 %) account for only a minor fraction of the locally observed wind direction each. Air masses associated with this cluster descended from the free troposphere less than 30 h prior to their arrival at the receptor site and had significant residence time over arid regions west of India. Consequently, they are associated with low relative and absolute humidity and do not bring rain. The medium westerly cluster is typically observed shortly before the arrival of a western disturbance.

The *fast westerly* cluster is observed only during winter, summer and post monsoon seasons and accounts for 7.7, 6.4 and 6.4 % of the air masses respectively. The cluster is associated with a strong subtropical jet stream poised over westerly troughs and shows higher than average wind speeds. The predominant local wind direction for this cluster is West to Northwest during all seasons (60 %) and katabatic winds from the north-northwest to east-southeast sector (30 %) account for most of the remainder. South westerly (6 %) and south easterly winds (4 %) account only for a minor fraction of the locally observed wind direction each. Due to the fact that air masses associated with this cluster descended from the free troposphere less than 30 h prior to their arrival at the receptor site and had significant residence time over arid regions west of India, they are associated with low relative and absolute humidity and do not bring rain. The fast westerly cluster is most frequently observed during winter and early summer season 2–3 days prior to the arrival of a western disturbance.

The *south easterly* cluster is associated with the passage of a western disturbance in winter and summer and with active spells of the monsoon during monsoon season and accounts for 19.3, 13.1 and 42.6 % of the flow respectively. It is generally not observed during post monsoon season. The western disturbance is responsible for most of the wintertime and summer time rain events (Table 1). During winter and summer season, the predominant local wind direction for this cluster is south easterly (38 %). Katabatic winds from the north-northwest to east-southeast sector account for 27 %, south westerly winds for 17 % and north westerly winds for 18 % of the locally observed

ACPD
15, 11409–11464, 2015

wind direction. Temperatures and wind speeds associated with this cluster are above average in winter and below average in summer. The relative and absolute humidity of air masses associated with this cluster are always high during both seasons. During monsoon season, the "Bay of Bengal branch" of the monsoon circulation brings warm and moist air masses to the receptor site. The absolute humidity is high and the highest total amount of rainfall is observed for this cluster. The predominant local wind direction for this cluster is south east (53 %). Katabatic winds from the north-northwest to east-southeast sector account for 24 %, south westerly winds for 12 % and north westerly winds for 11 % of the locally observed wind direction.

The *south westerly* cluster is associated with the passage of a western disturbance in winter and summer and with "break" spells of the monsoon during monsoon season and accounts for 3.4, 7.3 and 10.4 % of the flow respectively. It is not observed during post monsoon season. During winter and summer, the south westerly cluster is usually observed in association with a weakening western disturbance or at times when the centre of the low pressure system is above or close to the receptor site. The predominant local wind directions are west to northwest (42 %) and southeast (35 %). South westerly winds (13 %) and katabatic flow (10 %) account only for a minor fraction of the locally observed wind direction. During monsoon this cluster is associated with "break" spells. "Break" spells occur when the monsoon trough is located over the foothills of the Himalayas and the low level jet originating off the coast of Somalia enters the IGP through the Indus valley. The local wind direction is variable: 46 % south east, 21 % north west 21 % katabatic flow and 11 % south westerly winds. The absolute humidity of air masses associated with this cluster is high although rainfall events occur only rarely. However, extreme rainfall events are associated more frequently with this cluster.

Calm conditions (WS $< 1\,\mathrm{m\,s^{-1}}$) account for only 4.5, 2.5, 5.2 and 8.7 % of the total time during winter, summer, monsoon, post-monsoon season respectively. They occur more frequently at night (60 %) and less frequently during the day (40 %). The local

ACPD
15, 11409–11464, 2015

wind direction during periods with low wind speed is variable: 36 % south west, 33 % katabatic flow, 19 % south east and 12 % north west.

3.3 Impact of air mass transport on Particulate Matter (PM) mass loadings

To quantify the contribution of long range transport to particulate matter mass loadings at the receptor site we calculated the cluster average mass loadings of coarse and fine mode particulate matter at the receptor site (Fig. 9) and the enhancement of PM mass loadings above the levels observed for the "local" cluster which represents the regional background pollution in the North West IGP best (Table 2). The enhancement is expressed in % of the total PM mass loading observed for the respective cluster. We determined whether the differences in PM mass loadings between the different clusters are significant using Levene's test for homogeneity of variance based on means and used the pair wise comparison based on Tukey's studentised HSD test (Honestly Significant Differences) for assessing the statistical significance of the difference of the mean for each pair of clusters and each season (Table 3).

3.3.1 Winter season

During winter season both long range transport from the west and south west and local pollution episodes lead to enhanced coarse mode PM mass loadings (Table 2). The contribution of long range transport to coarse mode particulate mass loadings varies from 9 % for the south westerly cluster to 28 % for the medium westerly cluster. Local pollution episodes contribute 14 % on an average to the coarse mode PM observed under calm conditions.

Despite the fact that the average coarse mode PM varies from 45 $\mu g\,m^{-3}$ for the south easterly cluster to 66 $\mu g\,m^{-3}$ for the medium westerly cluster (Table 3) the difference of the average is not statistically significant for any of the cluster pairs due to the high intra-cluster variance of coarse mode PM during winter season. Two sources contribute prominently to coarse mode PM mass loading during winter: aqueous phase

ACPD
15, 11409–11464, 2015

oxidation of gas phase precursors and dust. Figure 10 shows the correlation of CO with coarse mode PM ($PM_{10-2.5}$) as a function of meteorological conditions. Aqueous phase oxidation of gas phase precursors emitted during combustion leads to a high degree of correlation between coarse mode particulate matter and CO at high relative humidity (> 70 %, $r = 0.55$), while dust, both dust from long range transport and locally suspended dust, contributes significantly to coarse mode PM at RH < 50 % and high wind speeds (Fig. 10). The complex interplay of meteorology dependent emissions and oxidation leads to high intra-cluster variance of PM mass loadings and obscures the contribution of long range transport to PM levels.

The influence of wet scavenging on PM mass loadings, however, is statistically significant. During rain events, coarse mode PM mass loadings drop to 30 $\mu g\,m^{-3}$ under calm conditions (–47 %), 13 $\mu g\,m^{-3}$ for the local cluster (–72 %) and 11 $\mu g\,m^{-3}$ for the south easterly cluster (–78 %) and the magnitude of the drop depends only weakly on the total amount of rainfall. Fine PM mass loadings drop to 73 $\mu g\,m^{-3}$ under calm conditions (–48 %), 80 $\mu g\,m^{-3}$ for the local cluster (–27 %) and 15 $\mu g\,m^{-3}$ for the south easterly cluster (–80 %). This clearly demonstrates the profound influence of wet scavenging on fine mode PM mass loadings during winter. The percent decrease in fine mode PM mass loadings during rain events scales perfectly linearly with the total rainfall for each cluster (1.3 % decrease in $PM_{2.5}$ per mm of rainfall, $r^2 = 0.99$). The fact that the drop in coarse mode PM is independent of the total amount of rain while the drop in fine mode PM strongly depends on the total amount of rainfall could be an indicator that during winter time, soluble coarse mode PM (large salts) plays a crucial role in initiating rainfall as giant cloud condensation nuclei, while fine mode PM is mostly scavenged by below cloud scavenging.

For fine mode PM, local pollution episodes lead to the highest enhancements in fine mode PM mass loadings (22 %). Long range transport from the west contributes only moderately to fine mode PM (7 and 13 % for the medium westerly and slow westerly cluster respectively).

ACPD
15, 11409–11464, 2015

The highest fine mode PM mass loadings are observed under calm conditions during local pollution episodes (141 $\mu g\,m^{-3}$). The enhancement is significant when compared to the south-easterly (72 $\mu g\,m^{-3}$) south westerly (101 $\mu g\,m^{-3}$) and fast westerly cluster (100 $\mu g\,m^{-3}$). When only dry days are considered, the difference between local pollution episodes (146 $\mu g\,m^{-3}$ on dry days) and the local cluster (110 $\mu g\,m^{-3}$ on dry days), which represents the regional air pollution also becomes significant (Table 3).

The lowest fine mode PM mass loadings are observed for the south-easterly cluster (72 $\mu g\,m^{-3}$) – which is associated with the western disturbance and has significantly lower mass loadings than the local, slow westerly and medium westerly cluster. The fast westerly cluster which is usually observed shortly before a western disturbance establishes itself over India has the second lowest fine mode mass loadings (100 $\mu g\,m^{-3}$), though the difference is not statistically significant with respect to the other clusters due to large intra-cluster variability in the fine mode PM mass loadings.

During winter-time, emission of fine mode particulate matter is driven by combustion. Correlation plots of fine PM with CO ($r^2 = 0.70$), acetonitrile, a biomass combustion tracer ($r^2 = 0.35$), benzene ($r^2 = 0.49$) and NO_2, a tracer for high temperature combustion, ($r^2 = 0.43$), Fig. 11) clearly indicate that at the receptor site combustion is the predominant source of winter time fine mode PM across all clusters. Due to low ambient temperatures in the winter months, in particular in the surrounding mountain regions, those who cannot afford electric heaters burn dry leaves, wood, coal, agricultural residues and cow dung often mixed with garbage to keep themselves warm. This practice prevails in entire South Asia and explains the simultaneous increase in fine mode PM and acetonitrile during winter season. High emissions of benzene have previously been observed during biomass combustion episodes in the region (Sarkar et al., 2013) and inefficient combustion in open fires or simple stoves is known to cause high PM mass loadings (Habib et al., 2004; Venkataraman et al., 2005; Massey et al., 2009; Akagi et al., 2011). While there is a clear correlation between both benzene and acetonitrile and $PM_{2.5}$, the lower r^2 for acetonitrile ($r^2 = 0.35$) compared to the higher r^2 for benzene ($r^2 = 0.49$) and CO ($r^2 = 0.70$) indicates that mixtures of fuels

ACPD
15, 11409–11464, 2015

with variable biomass content are used for domestic heating purposes. The scatter plot between $PM_{2.5}$ and benzene (Fig. 11) also seems to suggest that there may be regional preferences with respect to the fuel mixture as the emission ratios of the south easterly cluster usually fall below the fit line, while those for the south westerly cluster fall above it. The largest scatter and hence variation in fuel type is observed under calm conditions and for the local and slow westerly cluster.

The high mass loading of fine mode particulate matter coupled with the high relative humidity, which frequently reaches values above 75 %, in particular during the night, leads to the formation of persistent fog and haze during winter time. The uptake of water soluble organic and inorganic gas phase species into the aqueous phase and the subsequent chemical reactions result in a fine mode aerosol that contains a large mass fraction of water soluble inorganic species (Kumar et al., 2007) and acts as a very efficient CCN. Repeated fog processing also leads to the formation of coarse mode inorganic salt particles (Kulshrestha et al., 1998; Kumar et al., 2007). Kaskaoutis et al. (2013) reported a bi-modal volume size distribution for wintertime aerosol in Kanpur with a first, higher peak between 200–300 nm and a second peak between 3–4 µm optical equivalent diameter. The ratio of coarse mode to fine mode PM observed at our site agrees well with the ratio of coarse mode to fine mode PM observed in their study. Kulshrestha et al. (1998) reported a bimodal size distribution peaking at 1 and 5 µm aerodynamic equivalent diameter for wintertime aerosol in Agra and found ammonium sulphates, ammonium nitrate and potassium sulphate dominated water soluble salts in the fine mode while sulphates, nitrates and chlorides of sodium, calcium and magnesium dominated coarse mode aerosol. Dey and Tripathi (2007) reported that in wintertime in Kanpur more than 75 % of coarse mode particulate matter consisted of water soluble salts and only less than 25 % of coarse mode PM consisted of mineral dust. Their findings are in line with our observations that aqueous phase processing of gas phase precursors is responsible for a significant fraction of coarse mode PM during winter season (Fig. 10).

Discussion Paper | Discussion Paper | Discussion Paper | Discussion Paper |

ACPD

15, 11409–11464, 2015

Contribution of long-range transport to PM mass loading in the NW-IGP

H. Pawar et al.

3.3.2 Summer season

During summer season long range transport from the west and south west contributes significantly to enhanced coarse mode PM mass loadings (Table 2). Long range transport contributes approximately 30 % to coarse mode PM in air masses associated with the south westerly, slow westerly and medium westerly cluster each and 57 % to coarse mode PM in air masses associated with the fast westerly cluster.

Air masses associated with the south easterly cluster (50 $\mu g\,m^{-3}$; Fig. 9) show significantly lower coarse mode PM mass loadings compared to south westerly, slow westerly, medium and fast westerly clusters and also compared to the local air masses observed under calm conditions. Only the difference with respect to the local cluster (80 $\mu g\,m^{-3}$), which represents regional air masses is not significant, mainly due to the high variance of coarse mode PM mass loadings of air masses attributed to the local cluster. The variance is caused by convective dust storms (Joseph, 1982). It is very interesting to note that air masses that have crossed the entire, densely populated IGP show the lowest PM mass loadings even when compared with the local cluster, which represents regional air masses or when compared to air masses representing a local fetch region observed under calm conditions (75 $\mu g\,m^{-3}$). This is true during both rain events and on dry days.

The highest cluster average is observed for the fast westerly cluster (184 $\mu g\,m^{-3}$). The coarse mode PM ($PM_{10-2.5}$) mass loadings for this cluster is significantly enhanced above the coarse mode PM mass loadings observed in all other clusters and under calm conditions (Table 3) and 57 % of the average PM mass is due to long range transport for this cluster. The coarse PM enhancement for the fast westerly cluster is associated with dust storms originating in the Middle East that reach our site from the West (Pandithurai et al., 2008).

The slow and medium westerly cluster and south westerly cluster show enhanced coarse mode PM ($PM_{10-2.5}$) mass loadings as well, though the difference is statistically significant only with respect to the south easterly cluster (Table 2). PM enhancements

ACPD
15, 11409–11464, 2015

for the south westerly cluster are associated with dust storms originating from the Thar Desert (Sharma et al., 2012) or the Arabian Peninsula that reach our site through the Indus valley.

During summer season, maximum rainfall is observed for the south-easterly, local cluster, south-westerly and slow westerly cluster in descending order of the absolute rainfall amount. Even when rain events, characterized by average coarse mode PM mass loadings of 50 $\mu g\,m^{-3}$ (−38 % in average $PM_{10-2.5}$ mass loading), 29 $\mu g\,m^{-3}$ (−41 % in average $PM_{10-2.5}$ mass loading) and 60 $\mu g\,m^{-3}$ (−50 % in average $PM_{10-2.5}$ mass loading) for the local, south-easterly and slow westerly cluster respectively and 62 $\mu g\,m^{-3}$ (−15 % in average $PM_{10-2.5}$ mass loading) for periods of calm are removed, the differences outlined above remain significant. The south-westerly cluster brings moisture from the Arabian Sea but also dust from the Arabian peninsula (Pease et al., 1998) consequently the average coarse mode PM during rain is comparable to the average coarse mode PM on dry days. It is interesting to note, that the slow westerly cluster shows an increment in fine PM values on rainy days (95 $\mu g\,m^{-3}$) as compared to dry days (84 $\mu g\,m^{-3}$) indicating that rainfall for this cluster is associated with convective dust storms.

For fine mode particulate matter, the slow westerly (84 $\mu g\,m^{-3}$) cluster shows significantly (Table 3) enhanced fine PM mass loadings and approximately 31 % of the fine PM for this cluster is contributed by transport from the west (Table 2). For the slow westerly cluster the differences are significant with respect to the south-easterly cluster (42 $\mu g\,m^{-3}$), south westerly (65 $\mu g\,m^{-3}$), local (58 $\mu g\,m^{-3}$) and medium westerly cluster (60 $\mu g\,m^{-3}$; Fig. 9). Local pollution episodes lead to a 13 % increase above the regional $PM_{2.5}$ background. For the fast westerly cluster (73 $\mu g\,m^{-3}$) 20 % of the fine mode PM is contributed by long range transport but the difference is only significant with respect to the south easterly cluster.

Just like for coarse mode PM, the lowest fine mode PM mass loadings are observed for the south easterly cluster. The difference is significant with respect to the south westerly, slow westerly and fast westerly cluster and with respect to the local pollu-

ACPD
15, 11409–11464, 2015

tion episodes observed under calm conditions. (Table 3). Overall fine mode PM mass loadings in summer are lower than during winter time.

During summer season the comparison of the emission ratios of acetonitrile, benzene, CO and NO_2 with fine mode particulate matter pattern indicate that several sources drive fine mode PM (Fig. 11). While there is still a reasonable correlation between CO and $PM_{2.5}$ ($r^2 = 0.39$) most other combustion tracers have a poor coefficient of correlation with $PM_{2.5}$. The scatter plots indicate a spread between at least two types of combustion. One type is characterized by high acetonitrile, benzene and NO_2 emissions but fairly low $PM_{2.5}$ mass loadings and is probably associated with wheat residue burning in Punjab, while the other type is characterized by lower benzene, NO_2 and acetonitrile mixing ratios but higher $PM_{2.5}$ mass. This second source is probably traffic, which in arid regions during summer season is responsible for significant (re)-suspension of dust in particular when wind speeds are high ($> 5\,m\,s^{-1}$).

Several authors reported that during summer season, coarse mode mineral dust with a single peak at 3–4 µm optical equivalent diameter dominates PM mass loadings in the IGP (Gautam et al., 2011; Kaskaoutis et al., 2013), however we find that fine mode particulate matter ($PM_{2.5}$) contributes almost equally to PM mass loadings and a significant fraction of $PM_{2.5}$ mass is still combustion derived. Only Jethva et al. (2005), reported a bimodal volume distribution for dust storms with one peak at 3–4 µm and a second peak at 1.5 µm which agrees well with our findings. The peak at 1.5 µm corresponds to the clay fraction of mineral dust and is frequently found to be strongly enriched in mineral dust plumes after extended long-range transport (Pöschl et al., 2010). At our site, we find that the coarse mode PM fraction in individual dust storm events varies between 45 and 92 %, with the highest coarse mode fraction typically recorded for dust storms originating in the Thar Desert. While during dust storms windblown dust contributes significantly to fine mode PM, $PM_{2.5}$ is usually dominated by combustion derived aerosols at our site (Fig. 11).

ACPD
15, 11409–11464, 2015

3.3.3 Monsoon season

During monsoon season the effect of wet scavenging of coarse mode PM mass loadings can be clearly seen in the low average coarse PM mass loadings. Qualitatively the average mass loading is anti-correlated with rainfall. The lowest coarse mode PM mass loadings are observed for the south easterly (22 $\mu g\, m^{-3}$) and south westerly (30 $\mu g\, m^{-3}$) cluster.

The slow westerly cluster (55 $\mu g\, m^{-3}$) shows significant enhancement over all other clusters and the calm periods. Long range transport from the west contributes approximately 30 % to enhanced coarse mode PM mass loadings in the slow westerly cluster (Table 2). However, when rain events are removed, the enhancement over the local cluster is no longer significant.

The local cluster (39 $\mu g\, m^{-3}$) shows enhancements over the south easterly cluster (22 $\mu g\, m^{-3}$) and periods with calm conditions (25 $\mu g\, m^{-3}$), however the enhancement over calm conditions is no longer significant when rain events with average coarse mode PM mass loadings of 22, 25 and 18 $\mu g\, m^{-3}$ respectively are removed from the three clusters (Fig. 9, Table 3).

During monsoon seasons, most coarse mode PM is derived from aqueous phase oxidation of gas phase precursors (Fig. 10), a process that is extremely efficient at RH > 75 % and the removal is controlled by wet scavenging. Dust storms contribute only occasionally to coarse mode PM.

For fine mode PM ($PM_{2.5}$), the south easterly cluster (26 $\mu g\, m^{-3}$) shows the lowest mass loadings. The difference is significant with respect to the local (43 $\mu g\, m^{-3}$) and slow westerly (51 $\mu g\, m^{-3}$) cluster (Fig. 9). The difference between south easterly cluster and calm pollution episodes become significant when only dry days with an average fine PM loading of 26 and 38 $\mu g\, m^{-3}$ respectively are considered (Table 3). The south-westerly cluster (29 $\mu g\, m^{-3}$), too, shows significantly lower fine mode PM when compared to the local (43 $\mu g\, m^{-3}$) and slow westerly (51 $\mu g\, m^{-3}$) cluster (Fig. 9). The slow westerly cluster shows significant enhancements of fine mode PM over all

ACPD
15, 11409–11464, 2015

other clusters except the local cluster and significant enhancement over calm periods. Transport contributes approximately 15 % to the fine mode PM for this cluster.

During monsoon season, the correlation of acetonitrile, benzene, CO and NO_2 with fine mode particulate matter indicates that multiple combustion sources drive fine mode PM (Fig. 11). While there is still correlation with CO ($r^2 = 0.44$), the coefficient of correlation of acetonitrile, benzene and NO_2 with $PM_{2.5}$ is low and the largest scatter due to biomass combustion derived $PM_{2.5}$ (associated with high acetonitrile, benzene and NO_2) is observed under calm conditions. $PM_{2.5}$ enhancements for the slow westerly cluster, on the other hand, are accompanied by low acetonitrile, benzene and NO_2 mixing ratios and are possibly caused by traffic.

3.3.4 Post monsoon season

During post monsoon season air masses reaching the site from the west (slow, medium and fast westerly cluster) show higher coarse PM mass loadings compared to the local cluster and air masses observed under calm conditions. Transport from the west contributes approximately 30 % each to the coarse mode PM mass loadings of the medium westerly and fast westerly cluster and approximately 10 % to the coarse mode PM mass loadings of the slow westerly cluster. The highest coarse mode PM is observed for the fast and medium westerly cluster.

The enhancement in coarse mode PM observed for the medium westerly cluster is statistically significant with respect to all other clusters, including the slow westerly cluster. The enhancement observed for the fast westerly cluster is statistically significant only with respect to the local cluster and calm conditions. Results remain significant even when rain events are removed from both.

Calm episodes have significantly lower coarse mode PM mass loadings ($43\,\mu g\,m^{-3}$) than the medium and fast westerly cluster indicating that local pollution episodes are not a significant source of coarse mode PM during post monsoon season, while the fetch region of the westerly clusters are.

ACPD
15, 11409–11464, 2015

The highest fine mode PM during post monsoon season is observed in the fast westerly cluster (97 $\mu g\, m^{-3}$) and transport contributes 18 % to the PM mass loading associated with this cluster (Table 2). Fine PM mass loadings for this cluster are significantly enhanced compared to calm conditions (76 $\mu g\, m^{-3}$) and the local (80 $\mu g\, m^{-3}$) and slow westerly cluster (70 $\mu g\, m^{-3}$). All differences discussed above remain significant when rain events are removed from the dataset and only dry days are considered. The second highest fine mode PM mass loadings are observed for the medium westerly cluster. Transport contributes 11 % to the PM mass loadings observed for this cluster and the source characteristics are similar to those observed for the fast westerly cluster (Fig. 11).

For the slow westerly and local cluster, smoke produced by crop residue burning is a major source of PM during this season as crop residue burning is practised in most of Punjab. Consequently all air masses reaching the receptor site from the West are impacted by this source. Air masses attributed to the slow westerly and local cluster and air masses observed under calm conditions show a clear enhancement in the PM to acetonitrile ratio above the line-fit representing the regional background on days when fresh crop residue burning plumes impact the site. Paddy residue burning leads to massive enhancements in acetonitrile and benzenoids (Sarkar et al., 2013) and equally large emissions of PM. Singh et al. (2010) reported monthly average SPM of 400–500 $\mu g\, m^{-3}$ for a village site near Patiala during October and November and monthly average SPM of 300–400 $\mu g\, m^{-3}$ at a suburban site (residential campus of Punjab University) during the same two months. At our suburban receptor site further downwind of the burning fields we find that PM_{10} generally ranges between 100 and 200 $\mu g\, m^{-3}$ and exceeds 200 $\mu g\, m^{-3}$ only during few episodes. Badrinath et al. (2009) showed that the crop residue burning smoke is mostly channelled into the IGP and Mishra and Shibata (2012) showed that the crop residue burning plumes impact sites as far downwind as Kanpur. During its journey, the smoke ages and aerosol size distributions are modified. Kaskaoutis and co-workers (2013) reported a bi-modal volume size distribution for post monsoon aerosol in Kanpur with a first, peak between 200–

300 nm and a second peak at 3–4 µm. In Kanpur, coarse mode aerosol exceeded fine mode PM (by a factor of 1.3), while at our receptor site closer to the burning fields fine mode PM exceeds coarse mode PM by a factor of 1.5. This indicates that during the 720 km journey from Punjab to Kanpur approximately 30 % of the fine particulate matter mass is transformed into coarse mode PM through repeated fog processing.

3.4 Impact of air mass transport on Particulate Matter (PM) exceedance events

The mean PM mass loadings of an air mass cluster represent a poor proxy for the number of days in exceedance of the national air quality standard. While individual pollution episodes with extremely high PM mass loadings such as dust storms can profoundly influence the cluster mean, they barely affect the number of exceedance days as such events are rare.

3.4.1 Winter season

During winter season emissions of gas phase precursors and particulate matter from local and regional sources are so high and the conversion of gas phase precursors to both $PM_{2.5}$ and PM_{10} is so efficient, that the NAAQS for both $PM_{2.5}$ and PM_{10} is exceeded 85 % (Fig. 12) of the days associated with the local cluster, i.e. air masses that had been confined over the NW-IGP three days prior to their arrival at the receptor site. Despite the fact that local pollution episodes and transport from the west do enhance PM_{10} mass loadings for the slow, medium and fast westerly cluster, both barely increase the fraction of days during which PM mass loadings exceed the NAAQS. The largest increase in the fraction of exceedance days is observed for the medium westerly cluster (from 85 to 89 % of the days associated with this synoptic scale transport both for $PM_{2.5}$ and PM_{10}) and the slow westerly cluster (from 85 to 91 % for PM_{10}). Significantly cleaner air masses with a lower fraction of exceedance events are usually associated with wet scavenging and/or air masses brought by a western disturbance (south-easterly cluster: 45 % of the days associated with this synoptic scale transport

ACPD
15, 11409–11464, 2015

both for $PM_{2.5}$ and PM_{10}; south-westerly cluster: 45 % of the days associated with this synoptic scale transport for $PM_{2.5}$ and 60 % for PM_{10}).

3.4.2 Summer season

During summer season, aqueous phase oxidation contributes less to $PM_{2.5}$ and PM_{10} mass loadings. Instead, PM mass is dominated by direct emissions, dust and photochemistry.

Despite frequent dust storms, exceedance events are less frequent during summer season than they are during winter season. The NAAQS for PM_{10} is exceeded 60 % of the days associated with the local cluster and the NAAQS for $PM_{2.5}$ is exceeded 40 % of the days associated with this synoptic scale transport. While dust storms – episodic events during which PM_{10} mass loadings can reach up to 3000 $\mu g\,m^{-3}$ – have a strong impact on the cluster mean in particular for the fast westerly cluster; they barely affect the number of exceedance events. This is particularly true for the fast and medium westerly cluster. Only for the south westerly cluster, dust storms increase the number of exceedance events compared to the local cluster from 60 to 80 % of the days associated with this synoptic scale transport for PM_{10} and from 40 to 50 % for $PM_{2.5}$. The highest increase in the number of exceedance events for $PM_{2.5}$ is observed for the slow westerly cluster, which is most strongly affected by wheat residue burning in Punjab. Wheat residue burning increases the number of exceedance events observed for the slow westerly cluster compared to the local cluster by 40 to 70 % of the days associated with this synoptic scale transport for $PM_{2.5}$ and from 60 to 75 % for PM_{10}.

The fraction of exceedance events for the south-easterly cluster, both for PM_{10} (34 % of the days associated with this synoptic scale transport) and $PM_{2.5}$ (20 % of the days associated with this synoptic scale transport) is associated with cleaner air masses reaching the receptor site from the eastern IGP.

ACPD
15, 11409–11464, 2015

3.4.3 Monsoon season

During monsoon season the number of exceedance events is controlled by the interplay of wet scavenging emissions and aqueous phase oxidation of gas phase precursors.

The frequency of $PM_{2.5}$ exceedance days for each cluster is anti-correlated with the total rainfall observed for the respective cluster. For PM_{10} the high number of PM_{10} exceedance events for the local cluster stands out. The local cluster shows a higher degree of cloudiness compared to the slow westerly cluster (indicated by the lower average daytime solar radiation, Table 2) and slightly less cloudiness compared to calm conditions. The number of rain events and the total amount of rainfall for the local cluster is higher compared to the rainfall and number of rain events observed for the slow westerly cluster. Under calm conditions, on the other hand, drizzle occurs very frequently. PM_{10} exceedance events seem to correlate with the number of precipitation-free cloud-cycles through which the aerosol is processed. Despite the fact that the number of rain events and the total amount of rainfall is higher for the local cluster and despite the fact that dust storms occasionally contribute to coarse mode PM mass loadings for the slow westerly cluster, the number of PM_{10} exceedance events for the local cluster is higher than the number of PM_{10} exceedance events for the slow westerly cluster.

3.4.4 Post monsoon season

During post-monsoon season crop residue burning coupled with aqueous phase oxidation of gas phase precursors again leads to a high frequency of exceedance events. The NAAQS for both $PM_{2.5}$ and PM_{10} is exceeded 65 and 70–75 % of the days associated with the synoptic scale transport for the local and slow westerly cluster and under calm conditions. Transport leads to an increase in the fraction of exceedance days to 73 and 94 % of the days associated with the synoptic scale transport for $PM_{2.5}$ both for the medium and fast westerly cluster respectively and to an increase in the fraction

Discussion Paper | Discussion Paper | Discussion Paper | Discussion Paper |
ACPD
15, 11409–11464, 2015
Contribution of long-range transport to PM mass loading in the NW-IGP
H. Pawar et al.

of exceedance days to 91 and 94 % of the days associated with the synoptic scale transport for the medium and fast westerly cluster respectively for PM_{10}.

4 Conclusions

We investigated the contribution of long range transport and local pollution episodes to the average coarse and fine mode PM mass loadings at our receptor site using two years of high temporal resolution data.

Long range transport from the west leads to significant enhancements in the average coarse mode PM mass loadings during all seasons. For the slow westerly cluster the contribution of long range transport to coarse mode PM varies between 9 % during post monsoon season and 34 % during summer season. For the medium westerly cluster the contribution of transport to coarse mode PM is 30 % during all seasons and for the fast westerly cluster the contribution of long range transport to coarse PM mass loadings varies between 18 and 57 %. For the south westerly cluster transport leads to enhanced coarse mode PM only during winter (9 %) and summer (34 %) season. During monsoon season PM mass loadings for this cluster are significantly lower compared to the local cluster thanks to the effect of wet scavenging. Local pollution episodes lead to enhanced coarse mode PM only during winter season. The south easterly cluster is associated with significantly lower coarse mode PM mass loadings during all seasons.

For fine mode PM the situation is more complex. The fast westerly cluster is associated with a 20 % increase in fine mode PM during summer and post monsoon season but cleaner air masses during winter season. The medium westerly cluster shows moderately enhance PM mass loadings during all seasons while slow westerly transport leads to enhanced $PM_{2.5}$ mass loadings during winter, summer and monsoon season but not during post monsoon season. The south easterly cluster is associated with significantly lower $PM_{2.5}$ mass loadings during all seasons.

The number of days during which PM mass loadings exceed the national ambient air quality standard (NAAQS) of 100 $\mu g\,m^{-3}$ for 24 h average PM_{10} and 60 $\mu g\,m^{-3}$ for

24 h average $PM_{2.5}$ (NAAQS, 2009), however is controlled by long range transport to a much lesser degree.

For the local cluster, which represents regional air masses (Source region: NW-IGP), the fraction of days during which the national ambient air quality standard (NAAQS) of $60\,\mu g\,m^{-3}$ for 24 h average $PM_{2.5}$ was exceeded varied between 22 % of the days associated with this synoptic scale transport during monsoon season and 85 % of the days associated with this synoptic scale transport during winter season; the fraction of days during which the national ambient air quality standard (NAAQS) of $100\,\mu g\,m^{-3}$ for the 24 h average PM_{10} was exceeded, varied between 37 % during monsoon season and 84 % during winter season.

Long range transport was responsible for both bringing air masses with a significantly lower fraction of exceedance days from the Eastern IGP and air masses with a moderate increase in the fraction of exceedance days from the West (Source region: Arabia, Thar desert, Middle East and Afghanistan). The south easterly cluster (Source region: Eastern IGP) is always associated with a significantly lower fraction of exceedance days and the south westerly cluster also leads to a lower fraction of exceedance days during winter and monsoon season.

Whenever long range transport increases the fraction of exceedance days the increase varies between a few percent and at most 30 %.

In order to bring PM mass loadings in compliance with the national ambient air quality standard (NAAQS) and reduce the number of exceedance days, mitigation of regional pollution sources needs to be given highest priority as the number of exceedance days for air masses associated with the source region NW-IGP is already extremely high.

Fine mode PM ($PM_{2.5}$) contributes most to PM exceedance events at a regional level and $PM_{2.5}$ mass loadings are largely controlled by combustion sources during all seasons. Primary emission and gas to particle conversion of gas phase precursors emitted during the combustion, both contribute to the final mass loadings in varying proportions.

ACPD
15, 11409–11464, 2015

To devise efficient mitigation strategies targeted at bringing down the number of PM exceedance events, a larger set of tracers needs to be incorporated and alternate source receptor modelling approaches e.g. PMF modelling targeted specifically towards identifying local and regional combustion sources contributing towards the emissions of PM and towards the emission gas phase aerosol precursors need to be adopted.

The Supplement related to this article is available online at doi:10.5194/acpd-15-11409-2015-supplement.

Acknowledgements. We thank the IISER Mohali Atmospheric Chemistry Facility for data and the Ministry of Human Resource Development (MHRD), India and IISER Mohali for funding the facility.

We thank the NOAA Air Resources Laboratory (ARL) for the provision of the HYSPLIT transport and dispersion model used in this study. We thank the ESA GlobCover 2009 Project (ESA 2010 and UCLouvain) for providing a high resolution land classification map of the region.

Harshita Pawar, Himanshu Sachan and Vinod Kumar gratefully acknowledge a DST Inspire fellowship, Boggarapu Prafulla Chandra acknowledges CSIR-JRF fellowship and Ruhani Arya gratefully acknowledges the IISER Mohali summer research fellowship program. Boggarapu Praphulla Chandra, Chinmoy Sarkar and Saryu Garg acknowledge a 6 month project assistant position funded by the DST – Max Planck Research Partner Group on “Tropospheric OH reactivity and VOC measurements”.

References

Abdalmogith, S. S., and Harrison, R. M.: The use of trajectory cluster analysis to examine the long-range transport of secondary inorganic aerosol in the UK, Atmos. Environ., 39, 6686–6695, doi:10.1016/j.atmosenv.2005.07.059, 2005. 11413

Agnihotri, C. and Singh, M.: Satellite study of western disturbances, Mausam, 33, 249–254, 1982. 11415

Akagi, S. K., Yokelson, R. J., Wiedinmyer, C., Alvarado, M. J., Reid, J. S., Karl, T., Crounse, J. D., and Wennberg, P. O.: Emission factors for open and domestic biomass burning for use in atmospheric models, Atmos. Chem. Phys., 11, 4039–4072, doi:10.5194/acp-11-4039-2011, 2011. 11428

Badarinath, K., Kharol, S. K., Sharma, A. R., and Krishna Prasad, V.: Analysis of aerosol and carbon monoxide characteristics over Arabian Sea during crop residue burning period in the Indo-Gangetic Plains using multi-satellite remote sensing datasets, J. Atmos. Sol.-Terr. Phy., 71, 1267–1276, 2009. 11435

Bell, M. L. and Davis, D. L.: Reassessment of the lethal London fog of 1952: novel indicators of acute and chronic consequences of acute exposure to air pollution, Environ. Health Persp., 109, 389–394, 2001. 11412

Bhat, G. S.: The Indian drought of 2002 a sub-seasonal phenomenon?, Q. J. Roy. Meteor. Soc., 132, 2583–2602, doi:10.1256/qj.05.13, 2006. 11417

Borge, R., Lumbreras, J., Vardoulakis, S., Kassomenos, P., and Rodríguez, E.: Analysis of long-range transport influences on urban PM_{10} using two-stage atmospheric trajectory clusters, Atmos. Environ., 41, 4434–4450, doi:10.1016/j.atmosenv.2007.01.053, 2007. 11413, 11419

Bow, S.-T.: Pattern Recognition: Application to Large Data-Set Problems, Marcel Dekker Inc., New York, 1984. 11420

Brankov, E., Rao, S. T., and Porter, P. S.: A trajectory-clustering-correlation methodology for examining the long-range transport of air pollutants, Atmos. Environ., 32, 1525–1534, doi:10.1016/S1352-2310(97)00388-9, 1998. 11420

Bryson, R. A. and Swain, A. M.: Holocene variations of monsoon rainfall in Rajasthan, Quaternary Res., 16, 135–145, doi:10.1016/0033-5894(81)90041-7, 1981. 11416

Buchanan, C. M., Beverland, I. J., and Heal, M. R.: The influence of weather-type and longrange transport on air particle concentrations in Edinburgh, U K., Atmos. Environ., 36, 5343–5354, 2002. 11413

Das, P. K.: Mean vertical motion and non-adiabatic heat sources over India during the monsoon, Tellus, 14, 212–220, doi:10.1111/j.2153-3490.1962.tb00132.x, 1962. 11415

Dey, S., and Tripathi, S.: Estimation of aerosol optical properties and radiative effects in the Ganga basin, northern India, during the wintertime, J. Geophys. Res.-Atmos., 112, D03203, doi:10.1029/2006jd007267, 2007. 11429

ACPD
15, 11409–11464, 2015

Contribution of long-range transport to PM mass loading in the NW-IGP

H. Pawar et al.

Dimri, A. P.: Impact of horizontal model resolution and orography on the simulation of a western disturbance and its associated precipitation, Meteorol. Appl., 11, 115–127, doi:10.1017/S1350482704001227, 2004. 11415
Dockery, D. W., Speizer, F. E., Stram, D. O., Ware, J. H., Spengler, J. D., and Ferris Jr., B. G.: Effects of inhalable particles on respiratory health of children, Am. Rev. Respir. Dis., 139, 587–594, 1989. 11412
Dockery, D. W., Pope, C. A., Xu, X., Spengler, J. D., Ware, J. H., Fay, M. E., Ferris Jr, B. G., and Speizer, F. E.: An association between air pollution and mortality in six US cities, New Engl. J. Med., 329, 1753–1759, 1993. 11412
Dorling, S. R., Davies, T. D., and Pierce, C. E.: Cluster analysis: a technique for estimating the synoptic meteorological controls on air and precipitation chemistry – Method and applications, Atmos. Environ. A-Gen., 26, 2575–2581, doi:10.1016/0960-1686(92)90110-7, 1992. 11420
Draxler, R. and Rolph, G.: HYSPLIT (HYbrid Single-Particle Lagrangian Integrated Trajectory) NOAA Air Resources Laboratory, College Park, MD, Model access via NOAA ARL READY Website, 2013. 11418
Draxler, R. R. and Hess, G.: An overview of the HYSPLIT_4 modelling system for trajectories, Aust. Meteorol. Mag., 47, 295–308, 1998. 11418
Englert, N.: Fine particles and human health – a review of epidemiological studies, Toxicol. Lett., 149, 235–242, 2004. 11411
Firket, J.: The cause of the symptoms found in the Meuse Valley during the fog of December, 1930, Bull. Acad. R. Med. Belg., 11, 683–741, 1931. 11412
Fleming, Z. L., Monks, P. S., and Manning, A. J.: Review: Untangling the influence of air-mass history in interpreting observed atmospheric composition, Atmos. Res., 104–105, 1–39, doi:10.1016/j.atmosres.2011.09.009, 2012. 11413
Gautam, R., Hsu, N. C., Tsay, S. C., Lau, K. M., Holben, B., Bell, S., Smirnov, A., Li, C., Hansell, R., Ji, Q., Payra, S., Aryal, D., Kayastha, R., and Kim, K. M.: Accumulation of aerosols over the Indo-Gangetic plains and southern slopes of the Himalayas: distribution, properties and radiative effects during the 2009 pre-monsoon season, Atmos. Chem. Phys., 11, 12841–12863, doi:10.5194/acp-11-12841-2011, 2011. 11432
Goswami, B. N.: Interannual variations of indian summer monsoon in a GCM: external conditions versus internal feedbacks, J. Climate, 11, 501–522, doi:10.1175/1520-0442(1998)011<0501:IVOISM>2.0.CO;2, 1998. 11416

ACPD
15, 11409–11464, 2015

Contribution of long-range transport to PM mass loading in the NW-IGP

H. Pawar et al.

Goswami, B. N., Venugopal, V., Sengupta, D., Madhusoodanan, M. S., and Xavier, P. K.: Increasing trend of extreme rain events over india in a warming environment, Science, 314, 1442–1445, doi:10.1126/science.1132027, 2006a. 11416

Goswami, B. N., Wu, G., and Yasunari, T.: The annual cycle, intraseasonal oscillations, and roadblock to seasonal predictability of the asian summer monsoon, J. Climate, 19, 5078–5099, doi:10.1175/JCLI3901.1, 2006b. 11416

Grivas, G., Chaloulakou, A., and Kassomenos, P.: An overview of the PM_{10} pollution problem, in the Metropolitan Area of Athens, Greece, assessment of controlling factors and potential impact of long range transport, Sci. Total Environ., 389, 165–177, doi:10.1016/j.scitotenv.2007.08.048, 2008. 11413

Habib, G., Venkataraman, C., Shrivastava, M., Banerjee, R., Stehr, J., and Dickerson, R. R.: New methodology for estimating biofuel consumption for cooking: atmospheric emissions of black carbon and sulfur dioxide from India, Global Biogeochem. Cy., 18, GB3007, doi:10.1029/2003gb002157, 2004. 11428

Jethva, H., Satheesh, S. K., and Srinivasan, J.: Seasonal variability of aerosols over the Indo-Gangetic basin, J. Geophys. Res., 110, D21204, doi:10.1029/2005JD005938, 2005. 11432

Joseph, P.: A tentative model of Andhi, Mausam, 33, 417–422, 1982. 11416, 11422, 11430

Joseph, P. and Raman, P.: Existence of low level westerly jet stream over peninsular India during July, Indian J. Meteorol. Geophys., 17, 407–410, 1966. 11416

Joseph, P. V. and Sijikumar, S.: Intraseasonal Variability of the Low-Level Jet Stream of the Asian Summer Monsoon, J. Climate, 17, 1449–1458, doi:10.1175/1520-0442(2004)017<1449:IVOTLJ>2.0.CO;2, 2004. 11416

Kappos, A. D., Bruckmann, P., Eikmann, T., Englert, N., Heinrich, U., Höppe, P., Koch, E., Krause, G. H., Kreyling, W. G., and Rauchfuss, K.: Health effects of particles in ambient air, Int. J. Hyg. Envir. Heal., 207, 399–407, 2004. 11411

Kaskaoutis, D., Sinha, P., Vinoj, V., Kosmopoulos, P., Tripathi, S., Misra, A., Sharma, M., and Singh, R.: Aerosol properties and radiative forcing over Kanpur during severe aerosol loading conditions, Atmos. Environ., 79, 7–19, 2013. 11429, 11432, 11435

Kassomenos, P., Vardoulakis, S., Borge, R., Lumbreras, J., Papaloukas, C., and Karakitsios, S.: Comparison of statistical clustering techniques for the classification of modelled atmospheric trajectories, Theor. Appl. Climatol., 102, 1–12, doi:10.1007/s00704-009-0233-7, 2010. 11419, 11420

Kaushik, C., Ravindra, K., Yadav, K., Mehta, S., and Haritash, A.: Assessment of ambient air quality in urban centres of Haryana (India) in relation to different anthropogenic activities and health risks, Environ. Monit. Assess., 122, 27–40, 2006. 11412

Kulshrestha, U. C., Saxena, A., Kumar, N., Kumari, K. M., and Srivastava, S. S.: Chemical composition and association of size-differentiated aerosols at a suburban site in a semi-arid tract of India, J. Atmos. Chem., 29, 109–118, doi:10.1023/A:1005796400044, 1998. 11429

Kumar, R., Srivastava, S., and Kumari, K. M.: Characteristics of aerosols over suburban and urban site of semiarid region in India: seasonal and spatial variations, Aerosol Air Qual. Res., 7, 531–549, 2007. 11429

Lang, T. J., and Barros, A. P.: Winter storms in the Central Himalayas, J. Meteorol. Soc. Jpn., 82, 829–844, doi:10.2151/jmsj.2004.829, 2004. 11416

Logan, W.: Mortality in the London fog incident, 1952, Lancet, 261, 336–338, 1953. 11412

Massey, D., Masih, J., Kulshrestha, A., Habil, M., and Taneja, A.: Indoor/outdoor relationship of fine particles less than 2.5 µm ($PM_{2.5}$) in residential homes locations in central Indian region, Build. Environ., 44, 2037–2045, 2009. 11428

Miller, L., Farhana, S., and Xu, X.: Trans-boundary air pollution in Windsor, Ontario (Canada), Procedia Environmental Sciences, 2, 585–594, doi:10.1016/j.proenv.2010.10.064, 2010. 11413

Mishra, A. K. and Shibata, T.: Synergistic analyses of optical and microphysical properties of agricultural crop residue burning aerosols over the Indo-Gangetic Basin (IGB), Atmos. Environ., 57, 205–218, 2012. 11435

Mohanraj, R. and Azeez, P.: Health effects of airborne particulate matter and the Indian scenario, Curr. Sci. India, 87, 741–748, 2004. 11412

Mooley, D.: The role of western disturbances in the production of weather over India during different seasons, Indian J. Meteor. Geophys., 8, 253–260, 1957. 11415

NAAQS: National Ambient Air Quality Standard 2009, The Gazette of India, Extraordinary, Kartika 27, 1931, Government of India, New Delhi, 2009. 11412

Nag, S., Gupta, A., and Mukhopadhyay, U.: Size distribution of atmospheric aerosols in Kolkata, India and the assessment of pulmonary deposition of particle mass, Indoor Built Environ., 14, 381–389, 2005. 11412

Nemery, B., Hoet, P. H., and Nemmar, A.: The Meuse Valley fog of 1930: an air pollution disaster, Lancet, 357, 704–708, 2001. 11412

ACPD
15, 11409–11464, 2015

Nyanganyura, D., Makarau, A., Mathuthu, M., and Meixner, F. X.: A five-day back trajectory climatology for Rukomechi research station (northern Zimbabwe) and the impact of large-scale atmospheric flows on concentrations of airborne coarse and fine particulate mass, S. Afr. J. Sci., 104, 43–52, 2008. 11413

Pandey, J. S., Kumar, R., and Devotta, S.: Health risks of NO_2, SPM and SO_2 in Delhi (India), Atmos. Environ., 39, 6868–6874, 2005. 11412

Pandithurai, G., Dipu, S., Dani, K., Tiwari, S., Bisht, D., Devara, P., and Pinker, R.: Aerosol radiative forcing during dust events over New Delhi, India, J. Geophys. Res.-Atmos., 113, D13209, doi:10.1029/2008jd009804, 2008. 11430

Pease, P. P., Tchakerian, V. P., and Tindale, N. W.: Aerosols over the Arabian Sea: geochemistry and source areas for aeolian desert dust, J. Arid Environ., 39, 477–496, 1998. 11431

Pisharoty, P. and Desai, B.: Western disturbances and Indian weather, Indian J. Meteorol. Geophys., 8, 333–338, 1956. 11415

Pope III, C.: Epidemiology of fine particulate air pollution and human health: biologic mechanisms and who's at risk?, Environ. Health Persp., 108, 713–723, 2000. 11412

Pope III, C. A., Thun, M. J., Namboodiri, M. M., Dockery, D. W., Evans, J. S., Speizer, F. E., and Heath Jr, C. W.: Particulate air pollution as a predictor of mortality in a prospective study of US adults, Am. J. Resp. Crit. Care, 151, 669–674, 1995. 11412

Pope III, C. A., and Dockery, D. W.: Health effects of fine particulate air pollution: lines that connect, J. Air Waste Manage., 56, 709–742, 2006. 11411

Pöschl, U., Martin, S. T., Sinha, B., Chen, Q., Gunthe, S. S., Huffman, J. A., Borrmann, S., Farmer, D. K., Garland, R. M., Helas, G., Jimenez, J. L., King, S. M., Manzi, A., Mikhailov, E., Pauliquevis, T., Petters, M. D., Prenni, A. J., Roldin, P., Rose, D., Schneider, J., Su, H., Zorn, S. R., Artaxo, P., and Andreae, M. O.: Rainforest aerosols as biogenic nuclei of clouds and precipitation in the Amazon, Science, 329, 1513–1516, doi:10.1126/science.1191056, 2010. 11432

Ramaswamy, C.: On the sub-tropical jet stream and its role in the development of large-scale convection, Tellus, 8, 26–60, 1956. 11416

Rao, P. S. and Sikka, D. R.: Intraseasonal variability of the summer monsoon over the North Indian Ocean as revealed by the BOBMEX and ARMEX field programs, Pure Appl. Geophys., 162, 1481–1510, doi:10.1007/s00024-005-2680-0, 2005. 11417

Sarkar, C., Kumar, V., and Sinha, V.: Massive emissions of carcinogenic benzenoids from paddy residue burning in North India, Curr. Sci. India, 104, 1703–1706, 2013. 11428, 11435

Schrenk, H. H., Heimann, H., Clayton, G. D., Gafafer, W., and Wexler, H.: Air Pollution in Donora, Pa. Epidemiology of the Unusual Smog Episode of October 1948, Preliminary Report, Public Health Bulletin, no 306, Washington, D.C. : Federal Security Agency, Public Health Service, Bureau of State Services, Division of Industrial Hygiene, 173 pp., 1949. 11412

Schwartz, J.: Air pollution and daily mortality: a review and meta analysis, Environ. Res., 64, 36–52, 1994. 11412

Sharma, D., Singh, D., and Kaskaoutis, D.: Impact of two intense dust storms on aerosol characteristics and radiative forcing over Patiala, northwestern India, Advances in Meteorology, 2012, 956814, doi:10.1155/2012/956814, 2012.

Shy, C. M.: Epidemiologic evidence and the United States air quality standards, Am. J. Epidemiol., 110, 661–671, 1979. 11412

Sikka, D.: Evaluation of monitoring and forecasting of summer monsoon over India and a review of monsoon drought of 2002, Proceedings – Indian National Science Academy Part A, 69, 479–504, 2003. 11417

Sikka, D. R. and Gadgil, S.: On the maximum cloud zone and the ITCZ over Indian, longitudes during the Southwest Monsoon, Mon. Weather Rev., 108, 1840–1853, doi:10.1175/1520-0493(1980)108<1840:OTMCZA>2.0.CO;2, 1980. 11416

Singh, N., Mittal, S. K., Agarwal, R., Awasthi, A., and Gupta, P. K.: Impact of rice crop residue burning on levels of SPM, SO_2 and NO_2 in the ambient air of Patiala (India), Int. J. Environ. An. Ch., 90, 829–843, 2010. 11435

Sinha, V., Kumar, V., and Sarkar, C.: Chemical composition of pre-monsoon air in the Indo-Gangetic Plain measured using a new air quality facility and PTR-MS: high surface ozone and strong influence of biomass burning, Atmos. Chem. Phys., 14, 5921–5941, doi:10.5194/acp-14-5921-2014, 2014. 11414

Stohl, A.: Trajectory statistics – a new method to establish source-receptor relationships of air pollutants and its application to the transport of particulate sulfate in Europe, Atmos. Environ., 30, 579–587, doi:10.1016/1352-2310(95)00314-2, 1996. 11413

Stohl, A.: Computation, accuracy and applications of trajectories – a review and bibliography, Atmos. Environ., 32, 947–966, doi:10.1016/S1352-2310(97)00457-3, 1998. 11413

Venkataraman, C., Habib, G., Eiguren-Fernandez, A., Miguel, A., and Friedlander, S.: Residential biofuels in South Asia: carbonaceous aerosol emissions and climate impacts, Science, 307, 1454–1456, 2005. 11428

Ware, J. H., Thibodeau, L. A., Speizer, F. E., Colóme, S., and Ferris Jr, B. G.: Assessment of the health effects of atmospheric sulfur oxides and particulate matter: evidence from observational studies, Environ. Health Persp., 41, 255–276, 1981. 11412

ACPD
15, 11409–11464, 2015

Title Page
Abstract | Introduction
Conclusions | References
Tables | Figures
◀| |▶
◀ ▶
Back | Close
Full Screen / Esc
Printer-friendly Version
Interactive Discussion

Table 1. Average of the locally measured meteorological parameters for daytime/nighttime for the different clusters and seasons.For solar radiation we provided the daytime average only. For rain we calculated the sum of the rainfall instead of the average and the numbers in brackets represent the number of rain events.

ACPD
15, 11409–11464, 2015

	Fast Westerly	Medium Westerly	Slow Westerly	Local	South Westerly	South Easterly	Calm
WINTER (Dec–Feb)							
T (°C)	18.9/8.5	17.7/9.4	17.5 / 9.3	17.7/9.8	15.6/12.7	18.3/12.0	16.6/10.4
RH (%)	43.6/82.5	49.5/79.6	50.0/79.5	53.7/79.9	57.8/74.5	57.2/77.8	62.2/79.7
Wind Speed ($m\,s^{-1}$)	7.0/5.0	8.2/3.2	5.7/3.0	5.4/3.5	5.4/6.0	6.9/4.8	0.8/0.7
Wind Direction	302/319	270/303	306/294	292/304	298/240	241/188	235/139
Absolute Humidity ($g\,m^{-3}$)	7.4 /7.2	7.9/7.3	7.8/7.3	8.5/7.6	8.1/8.6	9.4/8.5	9.2/7.9
Solar Radiation ($W\,m^{-2}$)	414	331	381	376	362	338	307
Rain (mm)	–	–	–	7.7 (2)	–	50.7 (11)	27.3 (8)
SUMMER (Mar–Jun)							
T (°C)	31.7/19.3	32.6/20.3	35.9/26.5	32.1/22.7	32.5/25.2	29.5/22.9	34.2/23.3
RH (%)	23.4/58.8	22.1/50.7	24.3/44.7	28.7/51.8	36.2/52.5	44.1/64.1	29.0/53.3
Wind Speed ($m\,s^{-1}$)	9.1/5.6	7.6/3.6	7.7/4.5	7.2/4.3	7.9/4.5	7.0/5.6	0.9/0.7
Wind Direction	312/308	306/124	288/280	298/264	182/135	171/152	209/186
Absolute Humidity ($g\,m^{-3}$)	8.1/10.3	8.0/9.4	10.3 /11.7	10.0/11.0	12.9/12.8	13.5/13.8	11.3/11.7
Solar Radiation ($W\,m^{-2}$)	633	607	593	586	519	569	548
Rain (mm)	–	–	8.5 (3)	28.5 (5)	18.6 (2)	35.8 (10)	27 (27)
MONSOON (Jul–Sep)							
T (°C)	–	–	32.9/25.6	32.4/26.3	30.6/26.0	31.3/27.1	32.3/26.5
RH (%)	–	–	50.5/80.1	57.5/82.0	68.0/85.2	64.9/81.8	61.7/83.6
Wind Speed ($m\,s^{-1}$)	–	–	8.5/4.5	6.4/3.2	5.4/4.1	6.3/4.2	0.8/0.7
Wind Direction	–	–	309/191	280/148	182/124	166/128	206/132
Absolute Humidity ($g\,m^{-3}$)	–	–	18.4/19.9	20.4/21.2	22.0/21.7	21.7/22.1	21.8/21.8
Solar Radiation ($W\,m^{-2}$)	–	–	565	515	430	472	499
Rain (mm)	–	–	0.4(1)	33.8(4)	74.1(3)	142.2 (9)	36 (29)
POST-MONSOON (Oct–Nov)							
T (°C)	23.3/12.8	23.6/12.9	28.0/18.2	27.3/17.3	–	–	28.1/17.4
RH (%)	35.7/72.9	22.3/74.2	34.1/64.2	34.9/67.7	–	–	34.6/68.0
Wind Speed ($m\,s^{-1}$)	6.3/2.9	9.2/3.9	5.5/2.7	5.3/2.6	–	–	0.7/0.7
Wind Direction	310/175	313/315	310/71	304/174	–	–	214/115
Absolute Humidity ($g\,m^{-3}$)	7.7/8.5	8.0/8.7	9.7/10.5	9.5/10.4	–	–	9.8/10.6
Solar Radiation ($W\,m^{-2}$)	409	417	447	422	–	–	461
Rain (mm)	–	–	–	3.1 (2)	–	–	0.8 (2)

ACPD
15, 11409–11464, 2015

Contribution of long-range transport to PM mass loading in the NW-IGP

H. Pawar et al.

Table 2. Lower limit for the contribution of long range transport and local pollution events to PM mass loadings in % of the total PM. "negative" indicates that the PM mass loadings are not enhanced compared to the local cluster, which represent the regional background levels.

	Fast Westerly	Medium Westerly	Slow Westerly	South Westerly	South Easterly	Calm
			$PM_{2.5}$			
Winter	Negative	7	13	Negative	Negative	22
Summer	20	4	31	10	Negative	13
Monsoon	Negative	Negative	15	Negative	Negative	Negative
Post-Monsoon	18	11	Negative	Negative	Negative	Negative
			$PM_{10-2.5}$			
Winter	18	28	22	9	Negative	14
Summer	57	27	34	34	Negative	Negative
Monsoon	Negative	Negative	29	Negative	Negative	Negative
Post-Monsoon	27	31	9	Negative	Negative	Negative

ACPD
15, 11409–11464, 2015

Table 3. Statistical significance of the difference of the mean for each pair of clusters. Values to the right of the principal diagonal denote significance among $PM_{10-2.5}$ pairs while values to the left of the principal diagonal denote significance among $PM_{2.5}$ pairs. Pair wise comparison based on Tukey's studentised HSD test (Honestly significant differences) test was used to assess the statistical significance of the difference of the mean for each pair of clusters and each season. Values in brackets indicate the statistical significance after all rain events were removed from the dataset.

	Calm	South Easterly	South Westerly	Local	Slow Westerly	Medium Westerly	Fast Westerly
WINTER (Dec–Feb)							
Calm	–						
South Easterly	3σ (3σ)	–					
South Westerly	1σ(1σ)		–				
Local	– (1σ)	1σ		–			
Slow Westerly		2σ (1σ)			–		
Medium Westerly		1σ				–	
Fast Westerly	1σ (1σ)						–
SUMMER (Mar–Jun)							
Calm	–						4σ (3σ)
South Easterly	2σ (2σ)	–	2σ (1σ)		2σ (1σ)	1σ (1σ)	4σ (4σ)
South Westerly		1σ (1σ)	–				1σ (1σ)
Local				–			4σ (3σ)
Slow Westerly		4σ (4σ)	1σ (1σ)	2σ (2σ)	–		1σ (1σ)
Medium Westerly		1σ			1σ (1σ)	–	2σ (2σ)
Fast Westerly		2σ (2σ)					–
MONSOON (Jul–Sep)							
Calm	–			1σ	3σ (2σ)		
South Easterly	– (1σ)	–		1σ (1σ)	4σ (3σ)		
South Westerly			–		2σ (1σ)		
Local		2σ (2σ)	2σ (1σ)	–	1σ		
Slow Westerly	2σ (1σ)	4σ (4σ)	3σ (2σ)		–		
Medium Westerly						–	
Fast Westerly							–
POST-MONSOON (Oct–Nov)							
Calm	–					3σ (3σ)	2σ (2σ)
South Easterly		–					
South Westerly			–				
Local				–		2σ (1σ)	1σ (1σ)
Slow Westerly					–	1σ (1σ)	
Medium Westerly					1σ (1σ)	–	
Fast Westerly	1σ (1σ)			1σ (1σ)	2σ (2σ)		–

ACPD
15, 11409–11464, 2015

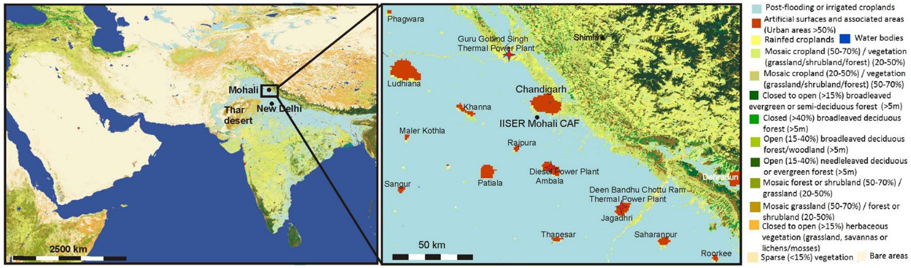

Figure 1. Left: location of Mohali on a land classification map (courtesy ESA GlobCover 2009 Project). The site is locatedin the north-west Indo-Gangetic plain, close to the forested slopes of the foothills of the Himalayan mountain range. Right: exact location of the measurement facility and its spatial relationship with respect to the nearby cities, the mountain range and potential local point sources of particulate matter.

ACPD
15, 11409–11464, 2015

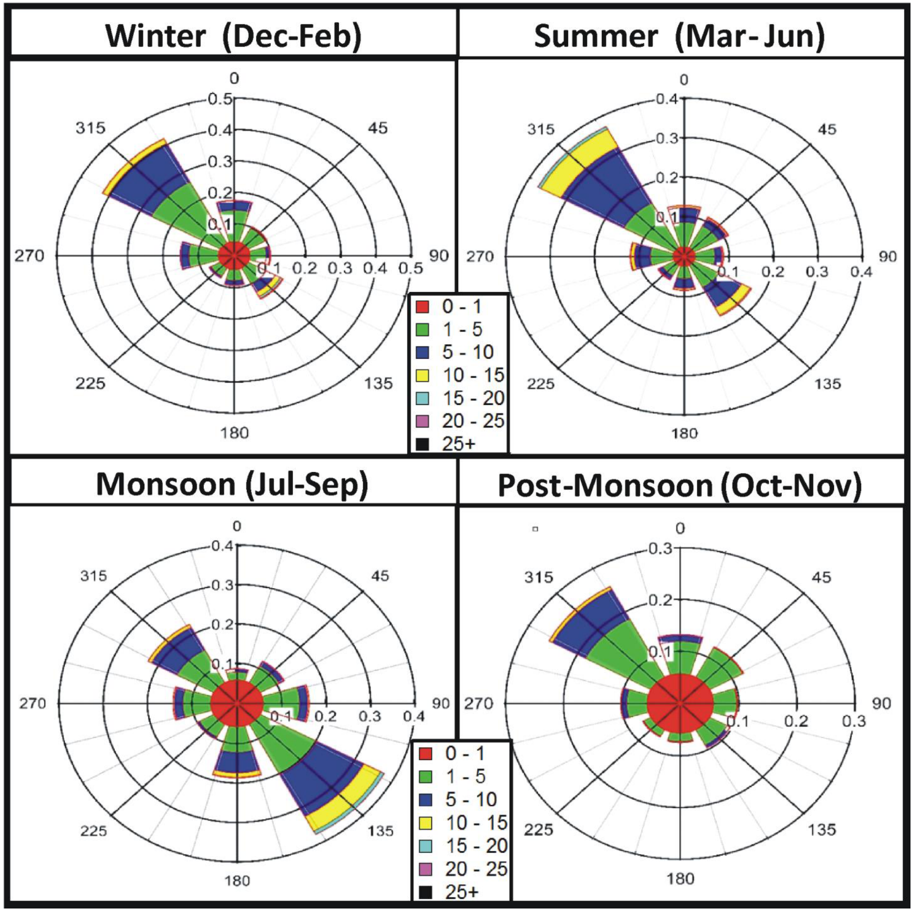

Figure 2. Wind rose plot for the measurement site for winter (December–February), summer (March–June), monsoon (July–September) and post-monsoon (October and November) season.

ACPD
15, 11409–11464, 2015

Contribution of long-range transport to PM mass loading in the NW-IGP

H. Pawar et al.

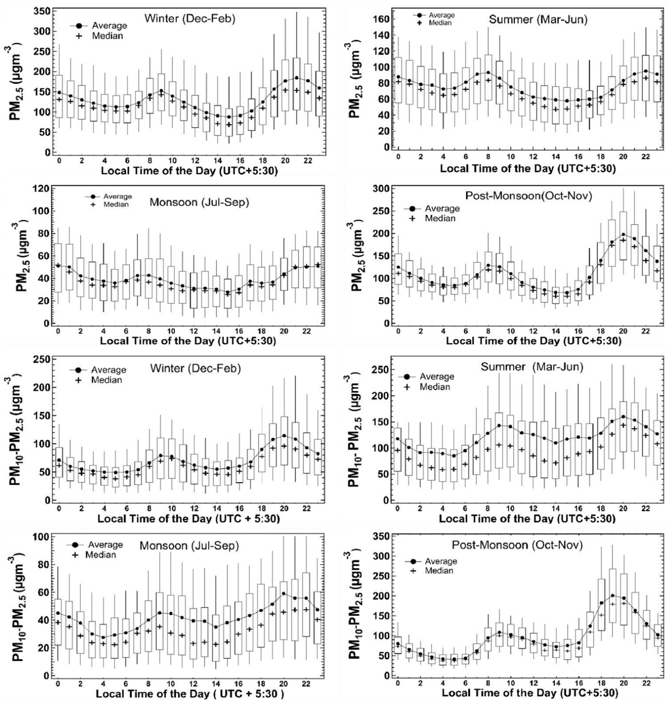

Figure 3. Diel box and whisker plots for fine mode (top four panels) and coarse mode (bottom four panels) particulate matter for winter, summer, monsoon and post monsoon season for the period November 2011 to August 2013 respectively. The box indicates the upper and lower quarter value; the cross indicates the median and the dots connected by lines provide the mean. The whiskers indicate the 5th and 95th percentile respectively. Periods of calm ($< 1\,\mathrm{m\,s^{-1}}$) have been excluded while preparing the graph.

ACPD
15, 11409–11464, 2015

Title Page
Abstract | Introduction
Conclusions | References
Tables | Figures
◀| |▶
◀ ▶
Back | Close
Full Screen / Esc
Printer-friendly Version
Interactive Discussion

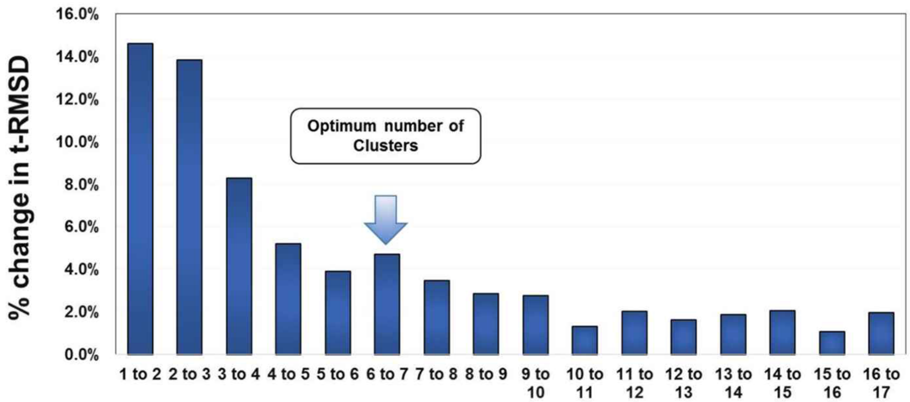

Figure 4. Percentage change in t-RMSD with increase in cluster number.

ACPD
15, 11409–11464, 2015

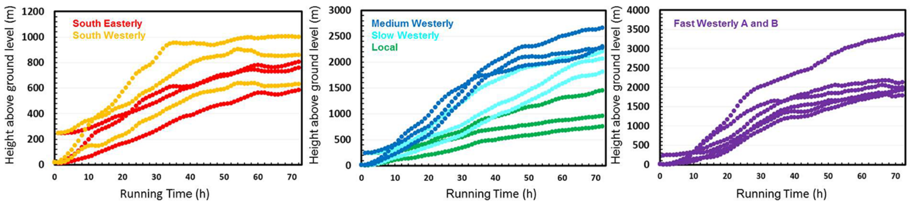

Figure 5. Mean height (a.g.l.) of all trajectories in an individual cluster as a function of trajectory running time (72 h) for trajectories arriving at 09:00 and 23:00 UTC.

ACPD
15, 11409–11464, 2015

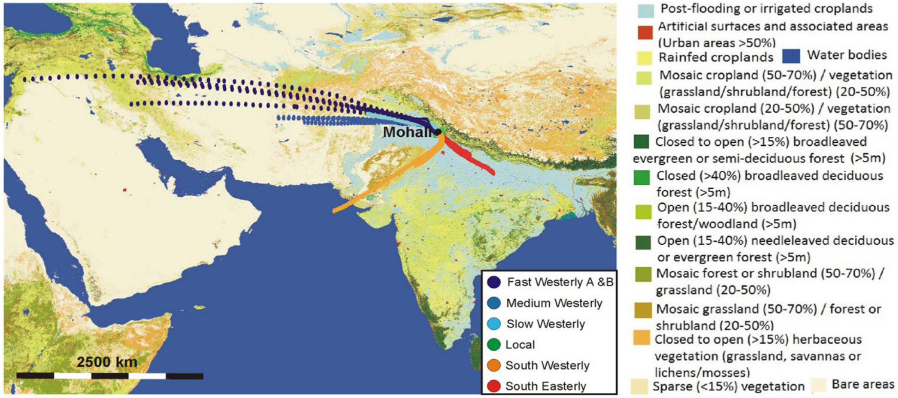

Figure 6. Average trajectory of seven clusters identified by k means clustering superimposed on a land classification map (courtesy ESA GlobCover 2009 Project). The length of each mean trajectory is 3 days and the distance between two successive data points represents a 1 h interval. For "Fast Westerly A and B" all 6 trajectory averages are shown in this figure.

ACPD
15, 11409–11464, 2015

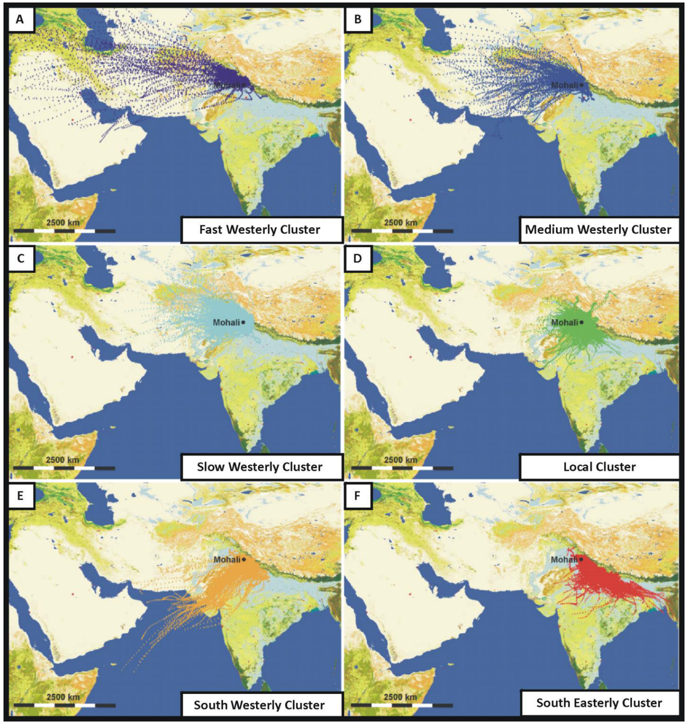

Figure 7. (**a–f**): All individual trajectories that contributed to each of the clusters, superimposed on a land classification map (courtesy ESA GlobCover 2009 Project). The length of each mean trajectory is 3 days and the distance between two successive data points represents a 1 h interval.

ACPD
15, 11409–11464, 2015

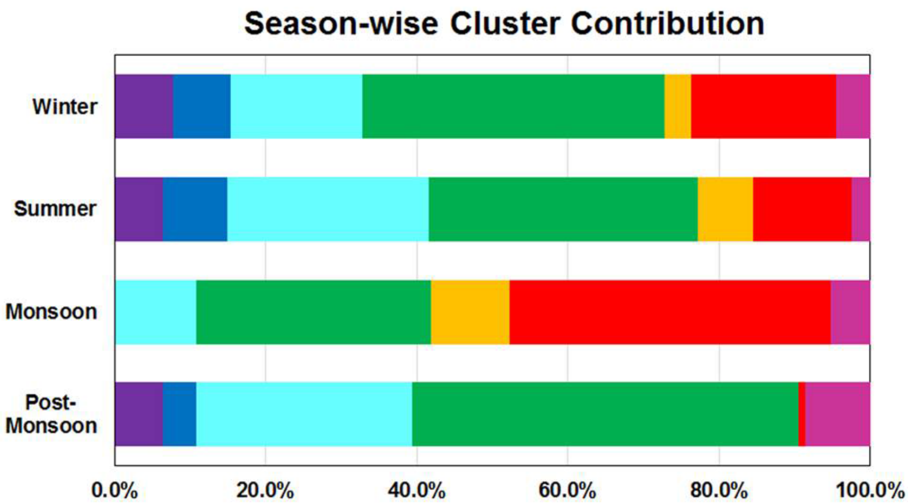

Figure 8. Contribution of individual clusters to air mass flow for all four seasons. Magenta: calm; red: south easterly cluster; orange: south westerly cluster; green: local cluster; light blue: slow westerly cluster; dark blue: medium westerly cluster; purple: fast westerly cluster.

ACPD
15, 11409–11464, 2015

Contribution of long-range transport to PM mass loading in the NW-IGP

H. Pawar et al.

ACPD
15, 11409–11464, 2015

Contribution of long-range transport to PM mass loading in the NW-IGP

H. Pawar et al.

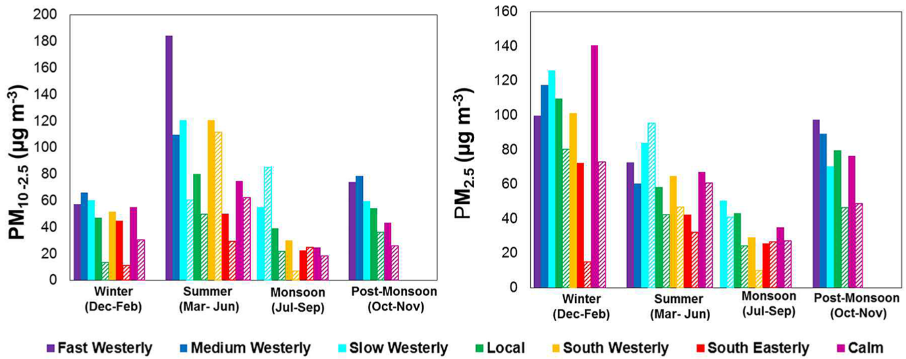

Figure 9. Mean coarse mode ($PM_{10-2.5}$) and fine mode ($PM_{2.5}$) mass loading for each air mass cluster and season at the IISER Mohali air quality station. Hatched bars indicate coarse mode and fine mode PM mass loadings observed during rain events.

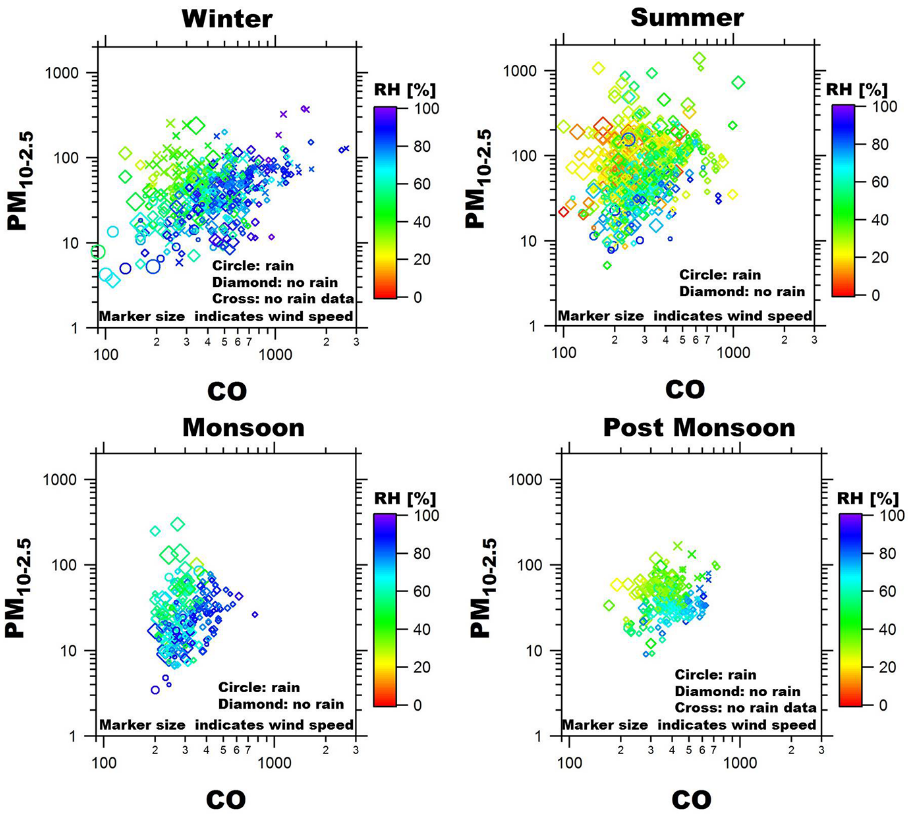

Figure 10. Dependence of coarse mode PM mass loadings on emission of gas phase precursors and meteorological parameters for the different seasons. The marker shape distinguishes PM mass loadings measured during rain events (circles) and under dry conditions (diamonds), data points obtained while the rain gauge was not working are marked with crosses. Marker size is proportional to wind speed. The smallest markers indicate WS $\leq 1\,\mathrm{m\,s^{-1}}$, the largest markers WS $\geq 15\,\mathrm{m\,s^{-1}}$. Markers are colour coded with relative humidity.

ACPD
15, 11409–11464, 2015

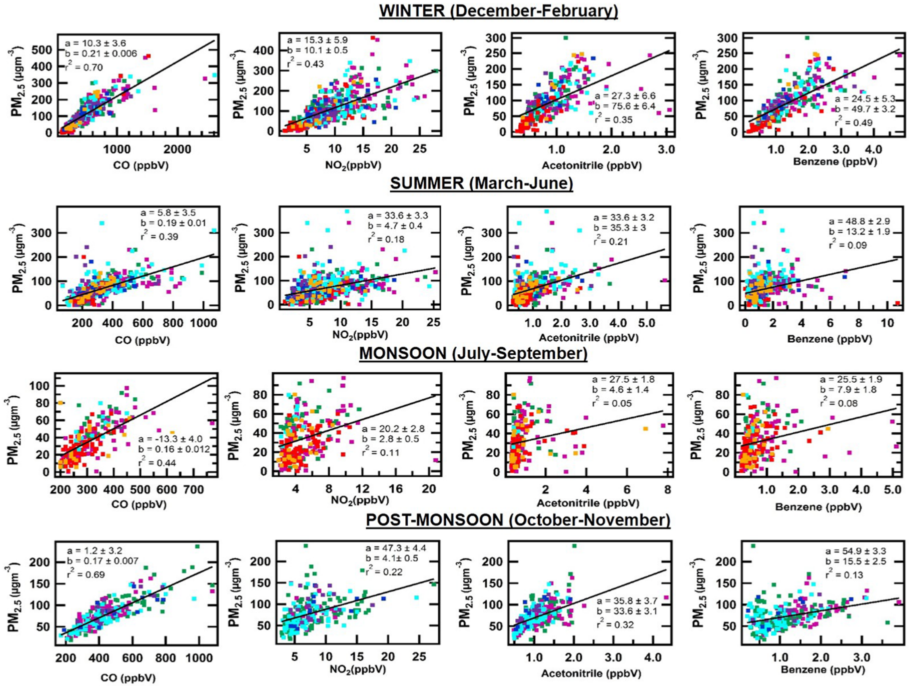

Figure 11. Scatter plots of fine mode PM with CO, acetonitrile, benzene and NO_2 for winter, summer, monsoon and post monsoon season.

ACPD
15, 11409–11464, 2015

Contribution of long-range transport to PM mass loading in the NW-IGP

H. Pawar et al.

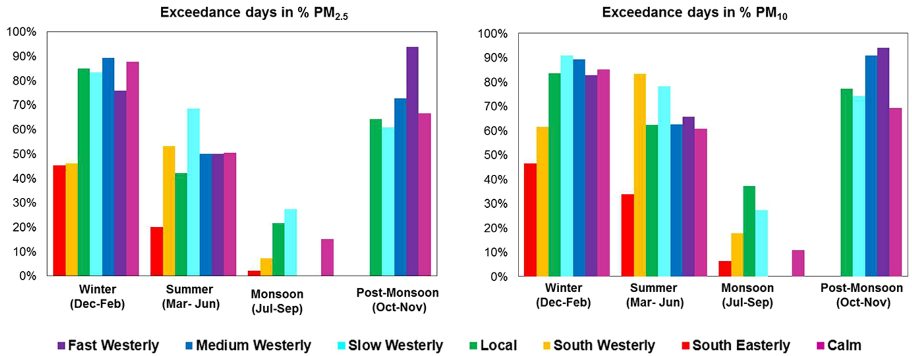

Figure 12. Percentage of days where the median coarse mode (PM_{10}) and fine mode ($PM_{2.5}$) mass loading (in $\mu g\,m^{-3}$) during the daytime/nighttime low exceeds the national ambient air quality standard for the 24 h average for each air mass cluster and season.

ACPD
15, 11409–11464, 2015

Contribution of long-range transport to PM mass loading in the NW-IGP

H. Pawar et al.